

Dilution impacts on smoke aging: Evidence in BBOP data

Anna L. Hodshire¹, Emily Ramnarine¹, Ali Akherati², Matthew L. Alvarado³, Delphine K. Farmer⁴, Shantanu H. Jathar², Sonia M. Kreidenweis¹, Chantelle R. Lonsdale³, Timothy B. Onasch⁵, Stephen R. Springston⁶, Jian Wang^{6,a}, Yang Wang^{7,b}, Lawrence I. Kleinman⁶, Arthur J. Sedlacek III⁶, Jeffrey R. Pierce¹

¹Department of Atmospheric Science, Colorado State University, Fort Collins, CO 80523, United States

²Department of Mechanical Engineering, Colorado State University, Fort Collins, CO 80523, United States

³Atmospheric and Environmental Research, Inc., Lexington, MA 02421, United States

⁴Department of Chemistry, Colorado State University, Fort Collins, CO 80523, United States

⁵Aerodyne Research Inc., Billerica, MA 01821, United States

⁶Environmental and Climate Sciences Department, Brookhaven National Laboratory, Upton, NY 11973, United States

⁷Center for Aerosol Science and Engineering, Washington University, St. Louis, MO 63130, United States

^aNow at Center for Aerosol Science and Engineering, Washington University, St. Louis, MO 63130, United States

^bNow at Department of Civil, Architectural and Environmental Engineering, Missouri University of Science and Technology, Rolla, Missouri 65409, United States

Correspondence to: Anna L. Hodshire (Anna.Hodshire@colostate.edu)

Abstract. Biomass burning emits vapors and aerosols into the atmosphere that can rapidly evolve as smoke plumes travel downwind and dilute, affecting climate- and health-relevant properties of the smoke. To date, theory has been unable to explain observed variability in smoke evolution. Here, we use observational data from the BBOP field campaign and show that initial smoke organic aerosol mass concentrations can help predict changes in smoke aerosol aging markers, number concentration, and number-mean diameter between 40-262 nm. Because initial field measurements of plumes are generally >10 minutes downwind, smaller plumes will have already undergone substantial dilution relative to larger plumes and have lower concentrations of smoke species at these observations closest to the fire. The extent to which dilution has occurred prior to the first observation is not a directly measurable quantity. We show that initial observed plume concentrations can serve as a rough indicator of the extent of dilution prior to the first measurement, which impacts photochemistry, aerosol evaporation, and coagulation. Cores of plumes have higher concentrations than edges. By segregating the observed plumes into cores and edges, we find evidence that particle aging, evaporation, and coagulation occurred before the first measurement. We further find that on the plume edges, the organic aerosol is more oxygenated while a marker for primary

Deleted: Hence

Deleted: .

42 biomass burning aerosol emissions has decreased in relative abundance than in the plume cores. Finally, we attempt to
43 decouple the roles of the initial concentrations and physical age, since emission by performing multivariate linear regression
44 of various aerosol properties (composition, size) on these two factors.

Deleted: .

Deleted: time

45 1 Introduction

46 Smoke from biomass burning is a major source of atmospheric primary aerosol and vapors (Akagi et al., 2011;
47 Gilman et al., 2015; Hatch et al., 2015, 2017; Jen et al., 2019; Koss et al., 2018; Reid et al., 2005; Yokelson et al., 2009),
48 influencing air quality, local radiation budgets, cloud properties, and climate (Carrico et al., 2008; O'Dell et al., 2019; Petters
49 et al., 2009; Ramnarine et al., 2019; Shrivastava et al., 2017), as well as the health of impacted communities (Ford et al.,
50 2018; Gan et al., 2017; Reid et al., 2016). Dilution of a smoke plume occurs as the plume travels downwind, mixing with
51 regional 'background' air, reducing the concentrations of smoke aerosols and vapors and potentially driving changes in the
52 physical and chemical properties of the emissions (Adachi et al., 2019; Akagi et al., 2012; Bian et al., 2017; Cubison et al.,
53 2011; Hecobian et al., 2011; Hodshire et al., 2019a, 2019b; Jolleys et al., 2012, 2015; Kononov et al., 2019; May et al.,
54 2015; Noyes et al., 2020; Sakamoto et al., 2015, Palm et al., 2020). Fires span an immense range in size, from small
55 agricultural burns, which may be only a few m² in total area and last a few hours, to massive wildfires, which may burn
56 10,000s of km² over the course of weeks (Andela et al., 2019). This range in size leads to variability in initial plume size and
57 extent of dilution by the time of the first measurement. Plumes can dilute unevenly, with edges of the plume mixing in with
58 surrounding air more rapidly than the core of the plume. Hence overall, these large, thick plumes dilute more slowly than
59 small, thin plumes for similar atmospheric conditions, as the cores of larger plumes are at a greater physical distance to the
60 background air, shielding them from dilution for longer (Akagi et al., 2012; Bian et al., 2017; Cubison et al., 2011; Hecobian
61 et al., 2011; Hodshire et al., 2019a, 2019b; Jolleys et al., 2012, 2015; Kononov et al., 2019; May et al., 2015; Sakamoto et
62 al., 2015, Lee et al., 2020, Garofalo et al., 2019). Variability in dilution leads to variability in the evolution of smoke
63 emissions as instantaneous plume aerosol concentrations will control shortwave radiative fluxes (and thus photolysis rates
64 and oxidant concentrations), gas-particle partitioning, and particle coagulation rates (Akagi et al., 2012; Bian et al., 2017;
65 Cubison et al., 2011; Hecobian et al., 2011; Hodshire et al., 2019a, 2019b; Jolleys et al., 2012, 2015; Kononov et al., 2019;
66 May et al., 2015; Sakamoto et al., 2015, Garofalo et al., 2019, Ramnarine et al., 2019; Sakamoto et al., 2016). Thus,
67 capturing variability in plume aerosol concentrations and dilution between fires and within fires can aid in understanding
68 how species change within the first few hours of emission for a range of plume sizes.

Deleted: the

Moved (insertion) [1]

Deleted:

Deleted: L

Moved up [1]: Plumes can dilute unevenly, with edges of the plume mixing in with surrounding air more rapidly than the core of the plume. Variability in dilution leads to variability in the evolution

69 The evolution of total particulate matter (PM) or organic aerosol (OA) mass from smoke has been the focus of
70 many studies, as PM influences both human health and climate. Secondary organic aerosol (SOA) production occurs through
71 oxidation of gas-phase volatile organic compounds (VOCs) that can form lower-volatility products that partition to the
72 condensed phase (Jimenez et al., 2009; Kroll and Seinfeld, 2008). SOA formation may also arise from heterogeneous and
73 multi-phase reactions in both the organic and aqueous phases (Jimenez et al., 2009; Volkamer et al., 2009). In turn, oxidant

82 concentrations depend on shortwave fluxes (Tang et al., 1998; Tie, 2003; Yang et al., 2009) and the composition of the
83 plume (Yokelson et al. 2009; Akagi et al. 2012; Hobbs et al. 2003; Alvarado et al. 2015). Smoke particles contain
84 semivolatile organic compounds (SVOCs) (Eatough et al., 2003; May et al., 2013), which may evaporate off of particles as
85 the plume becomes more dilute (Huffman et al. 2009; May et al. 2013; Garofalo et al. 2019; Grieshop et al. 2009), leading to
86 losses in total aerosol mass. Field observations of smoke PM and OA mass normalized for dilution (e.g. through a long-lived
87 tracer such as CO) report that for near-field (<24 hours) physical aging, net PM or OA mass can increase (Cachier et al.,
88 1995; Formenti et al., 2003; Liu et al., 2016; Nance et al., 1993; Reid et al., 1998; Vakkari et al., 2014, 2018; Yokelson et al.,
89 2009), decrease (Akagi et al., 2012; Hobbs et al., 2003; Jolleys et al., 2012, 2015; May et al., 2015), or remain nearly
90 constant (Brito et al., 2014; Capes et al., 2008; Collier et al., 2016; Cubison et al., 2011; Forrister et al., 2015; Garofalo et al.,
91 2019; Hecobian et al., 2011; Liu et al., 2016; May et al., 2015; Morgan et al., 2019; Sakamoto et al., 2015; Sedlacek et al.,
92 2018; Zhou et al., 2017). It is theorized that both losses and gains in OA mass are likely happening concurrently in most
93 plumes through condensation and evaporation (May et al. 2015; Hodshire et al. 2019; Hodshire et al. 2019; Bian et al. 2017;
94 Palm et al. 2020), with the balance between the two determining whether net increases or decreases or no change in mass
95 occurs during near-field aging. However, there is currently no reliable predictor of how smoke aerosol mass concentration
96 (normalized for dilution) may change for a given fire.

Deleted: n inert

97 Evolution of total aerosol number, size, and composition is critical for improving quantitative understanding of how
98 biomass burn smoke plumes impact climate. These impacts include smoke aerosols' abilities to both act as cloud
99 condensation nuclei (CCN) and to scatter/absorb solar radiation (Albrecht, 1989; Petters and Kreidenweis, 2007; Seinfeld
100 and Pandis, 2006; Twomey, 1974; Wang et al., 2008). Particles can increase or decrease in size as well as undergo
101 compositional changes through condensation or evaporation of more volatile compounds. In contrast, coagulation always
102 decreases total number concentrations and increases average particle diameter. Plumes with higher aerosol number
103 concentrations will undergo more coagulation than those with lower concentrations (Sakamoto et al., 2016).

Deleted: , each of which is determined by particle size and composition...

104 Fires in the western United States region are predicted to increase in size, intensity, and frequency (Dennison et al.,
105 2014; Ford et al., 2018; Spracklen et al., 2009; Yue et al., 2013). In response, several large field campaigns have taken place
106 in the last 7 years examining wildfires in this region (Kleinman et al., 2020; Garofalo et al. 2019; Palm et al., 2020). Here,
107 we present smoke plume observations from the Biomass Burning Observation Project (BBOP) campaign of aerosol
108 properties from five research flights sampling wildfires downwind in seven pseudo-Lagrangian sets of transects to
109 investigate the evolution of OA mass and oxidation state, aerosol number, and aerosol number mean diameter. A range of
110 initial (at the time of the first plume pass in the aircraft) plume OA mass concentrations were captured within these flights
111 and fast (1 second) measurements of aerosols and key vapors were taken. The time resolution of the data was fast enough to
112 segregate each transect into edge, core, or intermediate regions of the plume and examine aerosol properties within the
113 context of both the location within the plume (edge, core, or intermediate) and the initial OA mass loading of the given
114 location. The differences in aerosol loading serve as a proxy for differences in initial fire and plume sizes, mass fluxes, and
115 subsequent amount of dilution. The extent to which dilution has occurred prior to the first observation is not a measurable

Deleted: Being able to predict smoke aerosol mass, number, size, and composition accurately is an essential component in constraining the influence of fires on climate, air quality, and health.

Deleted: great

Deleted: that we have been able

Deleted:

25 quantity, and fire sizes and mass fluxes were not estimated as a part of the BBOP campaign. We create mathematical fits for
26 predicting OA oxidation markers and mean particle diameter given initial plume OA mass concentration and physical age
27 (time) of the smoke. These fits may be used to evaluate other smoke datasets and assist in building parameterizations for
28 regional and global climate models to better-predict smoke aerosol climate and health impacts.

29 2 Methods

30 The BBOP field campaign occurred in 2013 and included a deployment of the United States Department of Energy
31 Gulfstream 1 (G-1) research aircraft in the Pacific Northwest region of the United States (Kleinman and Sedlacek, 2016;
32 Sedlacek et al., 2018) from June 15 to September 13. We analyze five cloud-free BBOP research flights that had seven total
33 sets of across-plume transects that followed the smoke plume downwind in a Lagrangian manner (see Figs. S1-S6 for
34 examples; Table S1) from approximately 15 minutes after emission to 2-4 hours downwind (Kleinman and Sedlacek, 2016).
35 The G-1 sampling setup is described in (Kleinman and Sedlacek, 2016; Sedlacek et al., 2018; Kleinman et al., 2020).

36 Number size distributions were obtained with a Fast-integrating Mobility Spectrometer (FIMS), providing particle
37 size distributions nominally from approximately 20-350 nm (Kulkarni and Wang, 2006; Olfert and Wang, 2009); data was
38 available between 20-262 nm for the flights used in this study. A Soot Photometer Aerosol Mass Spectrometer (SP-AMS)
39 provided organic and inorganic (sulfate, chlorine, nitrate, ammonium) aerosol mass concentration of PM1 (sub-micron
40 aerosol) (Canagaratna et al. 2007), select fractional components (the fraction of the AMS OA spectra at a given mass-to-
41 charge ratio) (Onasch et al., 2012), and elemental analysis (O/C and H/C) (Aiken et al., 2008; Canagaratna et al., 2015).
42 Extended details on the SP-AMS are provided in Text S1 in the supplementary information, and a brief overview is given
43 here. The SP-AMS had its highest sensitivity between 70-500 nm, dropping to 50% of peak sensitivity by 1000 nm (Liu et
44 al. 2007). It was characterized to have a collection efficiency of 0.5 when the instrument's laser was off and 0.76 when the
45 instrument's laser was on during the BBOP campaign, and these corrections have been applied to the data. There is evidence
46 from other studies that the CE of the tungsten vaporizer (laser off mode) (Lim et al., 2019) and the laser vaporizer (laser on
47 mode, run nominally at 600° C) (Willis et al., 2014) to change as a function of chemical composition, rBC coating thickness,
48 size, and sphericity in laboratory studies (Middlebrook et al., 2012; Willis et al., 2014; Corbin et al., 2015; Massoli et al.,
49 2015; Collier et al., 2018) and in aircraft observations (Kleinman et al. 2007). Results pertinent to changes in CE due to
50 aging (including physical aging as well as chemical changes including oxidation, coating thickness, and sphericity) in smoke
51 plumes are scarce (see discussion in Kleinman et al., 2020). We assume these CEs for the laser on and off modes are
52 constant in space and time, which is a limitation of this study. We use the calculated f_{60} and f_{44} fractions (the unit mass
53 resolution mass concentration ratios of m/z 60 and 44 normalized by the total OA mass concentration) and O/C and H/C
54 elemental ratios of OA as tracers of smoke and oxidative aging. Elevated f_{60} values are indicative of "levoglucosan-like"
55 species (levoglucosan and other molecules that similarly fragment in the AMS) (Aiken et al., 2009; Cubison et al., 2011; Lee
56 et al., 2010) that are known tracers of smoke primary organic aerosol (POA) (Cubison et al., 2011). f_{44} the OA fractional

Deleted: s

Deleted:

Deleted: and

Formatted: Font: Not Italic, Not Superscript/ Subscript

60 component observed by the SP-AMS as the [high-resolution](#) ion fragment CO_2^+ as well as some acid groups, is a proxy for
61 SOA arising from oxidative aging (Alfarra et al., 2004; Cappa and Jimenez, 2010; Jimenez et al., 2009; Volkamer et al.,
62 2006). Fractional components f_{60} and f_{44} have been shown to decrease and increase with photochemical aging, respectively,
63 likely due to both evaporation and/or oxidation of semivolatile species that contribute to m/z 60 in the SP-AMS and addition
64 of oxidized species that contribute to m/z 44 in the SP-AMS (Alfarra et al., 2004; Huffman et al., 2009). O/C tends to
65 increase with oxidative aging (Decarlo et al., 2008) whereas H/C ranges from increasing to decreasing with oxidative aging,
66 depending on the types of reactions occurring (Heald et al., 2009). Changes in O/C and H/C (as well as changes in total OA
67 mass, number, f_{44} , and f_{60}) are also influenced by mixing of different air masses and co-oxidation of different VOC
68 precursors (Chen et al. 2015). Tracking H/C with aging may provide clues upon the types of reactions that may be occurring;
69 however, variable oxidation timescales can make inferences of this type difficult (Chen et al. 2015). A Single-Particle Soot
70 Photometer (SP2; Droplet Measurement Technologies) was used to measure refractory black carbon (BC) between 80-500
71 nm (Schwarz et al. 2010) through laser-induced incandescence (Moteki and Kondo, 2010; Schwarz et al., 2006). An Off-
72 Axis Integrated-Cavity Output Spectroscopy instrument (Los Gatos, Model 907) measured CO concentrations. An SPN1
73 radiometer (Badosa et al., 2014; Long et al., 2010) measured total shortwave irradiance. Kleinman et al. (2020) provides
74 extensive details for the BBOP instruments used in this work. The supporting information also includes more details on the
75 instruments used.

76 To determine the contribution to the concentration of species X from smoke emissions (ΔX), the background
77 concentration of X is subtracted off of the measured in-plume species concentrations. To correct for dilution, we normalize
78 ΔX by background-corrected CO (ΔCO), which is inert on timescales of near-field aging (Yokelson et al., 2009). Increases
79 or decreases of $\Delta X/\Delta \text{CO}$ along the Lagrangian flight path indicate whether the total amount of X in the plume has increased
80 or decreased (implying production or removal) since time of emission. The background concentration of X is determined as
81 a regional average of the observed out-of-plume concentrations of X. To avoid using smoke-impacted measurements we
82 apply a threshold of only using measurements of X that occur in regions that correspond to the lowest 10% of CO data. We
83 determine the lowest 10% of CO concentrations [for each flight during time periods with a similar altitude, latitude, and](#)
84 [longitude as the smoke plume.](#) We perform sensitivity calculations on our assumptions of background regions and discuss
85 them in Section 3.

86 Mass concentrations of O, H, and C are calculated using the O/C and H/C and OA data from the SP-AMS
87 (assuming all of the OA mass is from O, C, and H, [and we acknowledge that omitting lower-abundance atoms, such as S and](#)
88 [N, contributes to some errors in this assumption](#)), allowing us to calculate the background-corrected OA atomic ratios,
89 $\Delta \text{O}/\Delta \text{C}$, and $\Delta \text{H}/\Delta \text{C}$, following equation 1 (where X = O or H):

$$90 \frac{\Delta X}{\Delta C} = \frac{(X_{\text{in plume}} - X_{\text{out of plume}})}{(C_{\text{in plume}} - C_{\text{out of plume}})} \quad \text{Eq. 1}$$

91 We note that any non-linear changes in chemistry and composition between the plume and background will not perfectly
92 isolate the elemental factors in smoke. We also background-correct fractional f_{60} and f_{44} (using the mass concentrations of

Deleted:

Deleted: rom

Deleted: 1

96 m/z 60, m/z 44, and OA inside and outside of the plume), but we do not normalize by CO due to these values already being
97 normalized by OA, following equation 2 (where $f = f_{60}$ or f_{44}):

$$98 \Delta f = \frac{(f_{in} * OA_{in}) - (f_{out} * OA_{out})}{\Delta OA} \quad \text{Eq. 2}$$

99 We only consider data to be in-plume if the absolute CO \geq 150 ppbv. This threshold appears to be capturing clear plume
100 features as seen in the number concentration while excluding background air (Figs. S7-S11). We note that we use different
101 definitions of in-plume and background (i.e. the lowest 10% of absolute CO measurements) in order to provide a buffer
102 between the plume and background to ensure to the best of our abilities that we are capturing non-smoke impacted air for the
103 background and smoke-impacted air for in-plume cases. The regions of the lowest 10% of CO measurements always fall
104 under 150 ppbv (Figs. S7-S11). Similarly, we exclude the lowest 5% of CO data in the in-plume measurements in our
105 analyses to provide a further buffer between smoke-impacted and background air. We perform sensitivity analyses of our
106 results to our assumptions about background and in-plume values in Section 3. Figures S2-S6 indicate the locations of the
107 lowest 10% of CO for each flight.

108 From the FIMS, we examine the background-corrected, normalized number concentrations of particles with
109 mobility diameters between 40-262 nm, $\Delta N/\Delta CO$. This size range allows us to exclude potential influence of fresh
110 nucleation upon the total number concentrations. Occasionally, the background-corrected, normalized number concentration
111 in the FIMS size range between 20-40 nm increases by 1-2 orders of magnitude relative to typical plume conditions,
112 indicating possible nucleation events, primarily at the edges or in between smoke plumes (Figs. S7-S11). Smoke plumes
113 contain particles with diameters larger than 262 nm (Janhäll et al., 2009): thus, we cannot provide total number
114 concentrations, but we can infer how $\Delta N/\Delta CO$ within our observed size range evolves. We also obtain an estimate of how
115 the number mean diameter between 40-262 nm, \overline{D}_p , changes with aging through:

$$17 \overline{D}_p = \frac{\sum N_i * D_{p,i}}{\sum N_i} \quad \text{Eq. 3}$$

18 where N_i and $D_{p,i}$ are the number concentration and geometric mean diameter within each FIMS size bin, respectively.

19 All of the data are provided at 1 Hz and all but the SP-AMS fractional component data are available on the DOE
20 ARM web archive (<https://www.arm.gov/research/campaigns/aaf2013bbop>). As the plane traveled at approximately 100 m s⁻¹
21 on average, ~~the approximate spatial resolution of the data is~~ every 100 m across the plume. The plumes spanned from
22 approximately 5-50 km wide (Figs. S2-6). The instruments used here had a variety of time lags (all <10 seconds) relative to a
23 TSI 3563 nephelometer used as reference. The FIMS also showed additional smearing in flushing smoky air with cleaner air
24 when exiting the plume with maximum observed flushing timescales around 30 seconds, but generally less (Fig. S12). To
25 test if these lags impact our results, we perform an additional analysis where we only consider the first half of each in-plume
26 transect, when concentrations are generally rising with time (Figure S12-S13), and our main conclusions are unaffected. We
27

Field Code Changed

Deleted: <https://www.arm.gov/research/campaigns/aaf2013bbop>

Deleted: data were collected

30 do not test the impacts of other time lags and do not attempt to further correct the data for any time lags. Kleinman et al.
31 (2020) provides further information on instrument time delays during BBOP.

32 We use MODIS Terra and Aqua fire and thermal anomalies detection data to determine fire locations (Giglio et al.,
33 2006, 2008). We estimate the fire center to be the approximate center of all clustered MODIS detection points for a given
34 sampled fire (Figs. S1-S6). The true fire location at the time of sampling is likely different than the MODIS estimates,
35 depending on the speed of the fire front. To estimate the physical age of the plume, we use the estimated fire center as well
36 as the total FIMS number concentration to determine an approximate centerline of the plume as the smoke travels downwind
37 (an example is provided in Fig. S1). The centerline is subjectively chosen to approximately capture the most-concentrated
38 portion of each plume pass (as estimated using total aerosol number concentrations). We use the mean wind speed and this
39 estimated centerline to calculate an estimated physical age for each transect, and this physical age is assumed to be constant
40 across the transect, as plume crossings took between 50-500 seconds; however, transects that were not perfectly tangential to
41 the mean wind would have sampled different plume ages on the opposite sides of the plume. We did not propagate
42 uncertainty in fire location, wind speed, or centerline through to the physical age, which is a limitation of this study.

43 3 Results and discussion

44 As a case example, we examine the aging profiles of smoke from the Colockum fire during the first set of pseudo-
45 Lagrangian transects for flight 730b (Table S1). Figure 1 provides $\Delta OA/\Delta CO$, $\Delta BC/\Delta CO$, Δf_{60} , Δf_{44} , $\Delta H/\Delta C$, $\Delta O/\Delta C$,
46 $\Delta N/\Delta CO$, and $\overline{D_p}$ as a function of the estimated physical age; Figs. S14-S18 provides this information for the other pseudo-
47 Lagrangian transect flight sets studied. (Here, BC represents the refractory BC from the SP2; Sect. 2.) We have divided each
48 transect into four regions: between the 5-15 (edge), 15-50 (intermediate, outer), 50-90 (intermediate, inner), and 90-100
49 (core) percentile of ΔCO within each transect. (As discussed above, we exclude the lowest 5% in order to provide a buffer
50 between the plume edge and background air.) Note that in Figure 1 (and Figures S14-S18), the points represent the mean
51 values for each transect/percentile and do not include error bars for uncertainty in the mean or measurement uncertainty as
52 characterization of systematic variance (within plume percentiles) with age is beyond the scope of this study. Figures S2-S6
53 show the locations of these CO percentile bins for each transect of individual flights. Figure 1 shows the edge and core data,
54 both averaged per transect, and Figs. S14-18 provides all four percentile bins for each flight. These percentile bins correspond
55 with the thinnest (lowest CO mixing ratio) to thickest (highest CO mixing ratio) portions of the plume, respectively. If a fire
56 has uniform emissions ratios across all regions and dilutes evenly downwind, these percentile bins would correspond to the
57 edges, intermediate [outer](#) and [intermediate inner](#) regions, and the core of the diluting plume. We use this terminology in this
58 study but note that uneven emissions, mixing, and/or dilution lead to the percentile bins not physically corresponding to our
59 defined regions in some cases. We note that some plumes show more than one maxima in CO concentrations within a given
60 plume crossing, which implies that there may be more than one fire or fire front, and that these plumes from separate fires or
61 fronts are not mixing perfectly. Multiple maxima could also imply vertical variations in the location of the core of the

62 plumes that the flights did not capture. As well, in at least one of the fires (in flights ‘730a’ and ‘730b’), the fuels vary
63 between different sides of the fire, as discussed in Kleinman et al., (2020). However, the lowest two ΔCO bins tend towards
64 the physical edges of the plume, and the highest two tend more towards the physical center of the plume (Figs. S2-S6). We
65 do not know where the plane is vertically in the plume, which is a limitation as vertical location will also impact the amount
66 of solar flux able to penetrate through the plume.

67 Figure 1 shows that for this specific plume, $\Delta\text{OA}/\Delta\text{CO}$ and $\Delta\text{BC}/\Delta\text{CO}$ systematically vary little with age for both
68 the 5-15 and 90-100 percentile of ΔCO (p-values>0.5), yet both show non-systematic variability between transects. A true
69 Lagrangian flight with the aircraft sampling the same portion of the plume and no measurement artifacts (e.g. coincidence
70 errors at high concentrations) would have a constant $\Delta\text{BC}/\Delta\text{CO}$ for each transect set. This flight and other flights studied
71 here have variations in $\Delta\text{BC}/\Delta\text{CO}$ (Fig. 1; Figs. S14-S18), which may be indicative of deviations from a Lagrangian flight
72 path with temporal variations in emission and/or measurement uncertainties. The remaining variables plotted also show some
73 noise and few clear trends, but it is apparent that the transect-mean values 5-15 and 90-100 percentiles do show a separation
74 for some of the individual metrics, in particular Δf_{44} and $\Delta\text{O}/\Delta\text{C}$. In order to determine the existence or lack of trends for
75 these metrics, we spend the remainder of this study examining each metric from all of the pseudo-Lagrangian flights
76 together.

77

78 3.1 Organic aerosol aging: $\Delta\text{OA}/\Delta\text{CO}$, Δf_{60} , Δf_{44} , $\Delta\text{H}/\Delta\text{C}$, and $\Delta\text{O}/\Delta\text{C}$

79 Figure 2a-e shows available $\Delta\text{OA}/\Delta\text{CO}$, Δf_{60} , Δf_{44} , $\Delta\text{H}/\Delta\text{C}$, and $\Delta\text{O}/\Delta\text{C}$ edge and core data versus physical age for
80 each transect for each flight of this study. We color each line by the mean ΔOA within a ΔCO percentile bin from the
81 transect closest to the fire, $\Delta\text{OA}_{\text{initial}}$, in order to examine whether each variable ($\Delta\text{OA}/\Delta\text{CO}$, Δf_{60} , Δf_{44} , $\Delta\text{H}/\Delta\text{C}$, and $\Delta\text{O}/\Delta\text{C}$)
82 vary with $\Delta\text{OA}_{\text{initial}}$. (Some transects do not have data available for specific instruments.) As with Fig. 1, the points in Fig.
83 2 represent the mean values for each transect and percentile, and we do not include error bars as we do not attempt to
84 characterize systematic variance (within plume percentiles) with age in this study. We note that $\Delta\text{OA}_{\text{initial}}$ does not actually
85 represent the true initial emitted OA from each fire, but instead serves as a proxy for the general fire size, intensity, and
86 emission rate (as larger fires and fires with faster rates of fuel consumption per area will have larger mass fluxes than smaller
87 fires or fires with less fuel consumption per area, all else equal). Thus, $\Delta\text{OA}_{\text{initial}}$ and other “initial” metrics referred to in this
88 study are not to be taken as emission values and direct comparison to studies with direct emissions values is not appropriate,
89 as dilution and chemistry may occur before the initial flight transect, which we discuss further below. We show the 5-15
90 (edge) and 90-100 (core) ΔCO percentile bins in Fig. 2; Fig. S19 shows the same information for all four ΔCO percentiles.
91 We use the simple ‘edge’ and ‘core’ terminology throughout the following discussion but note that the 5-15 and 90-100 ΔCO
92 percentile bins do not necessarily correspond to the physical (spatial) edges and cores of each plume. They instead
93 correspond to the most CO-dense and least CO-dense portions of the plume. We also note that although some of the physical
94 ages appear to start at approximately 0 hours (e.g. over the fire), this is from a limitation of our physical age estimation

Deleted: more

Formatted: Font: Italic

Formatted: Font: Italic, Subscript

Formatted: Font: Italic

Formatted: Font: Italic, Subscript

96 method (Sect. 2), as no flights captured data before approximately 15 minutes after emission (Kleinman et al., 2016). Flights
97 with two sets of pseudo-Lagrangian transects ('726a' and '730b') have two separate lines in Fig. 2, one for each set. As well,
98 two transects for flight '809a' nearly overlap (Fig. S5), with the transect that is further from the fire occurring first in the
99 flight path, leading to an apparent slight decrease in physical age for the sequential transect (see, e.g., the white dashed line
00 in Fig. 2a).

01 Also included in Fig. 2 are the Spearman rank-order correlation tests (hereafter Spearman tests), which are tests for
02 monotonicity. The Spearman tests show correlation coefficients for each flight set (Table S1) with the initial ΔOA of a flight
03 set ($\Delta OA_{\text{initial}}$) against $\Delta OA/\Delta CO$, $\Delta f/\theta$, $\Delta f/44$, $\Delta H/\Delta C$, and $\Delta O/\Delta C$ as the smoke aerosol ages downwind. We also include
04 Spearman tests for the calculated physical age of the smoke for each flight set against these same variables. The R values are
05 labeled $R_{\Delta OA, \text{initial}}$ and R_{age} , respectively, in Fig. 2. We calculate these correlation coefficients separately for Figure 2 to
06 determine the strength and direction of association for each variable from $\Delta OA_{\text{initial}}$ or age alone (and whether the data are
07 correlated vs. anticorrelated with these predictors). To complement these independent correlation coefficients, we also
08 perform multivariate linear regressions (Eqns. 4 and 5 and Figure 3, discussed later) to explicitly decouple the influence of
09 the two predictors. For the correlations with $\Delta OA_{\text{initial}}$, all transects in a given pseudo-Lagrangian set of transects have the
10 same $\Delta OA_{\text{initial}}$ value; for flights with two pseudo-Lagrangian sets of transects, each set has its own $\Delta OA_{\text{initial}}$ value.
11 Correlating to $\Delta OA_{\text{initial}}$ provides an estimate of how the plume aerosol concentrations at the time of the initial transect
12 impact plume aging (aging both before and after this initial transect). We define the following categories of correlation for
13 the absolute value of R: 0.0-0.19 is 'very weak', 0.2-0.39 is 'weak', 0.4-0.59 is 'moderate', 0.6-0.79 is 'strong', and 0.8-1.0
14 is 'very strong' (Evans 1996).

15 As individual flights show scatter in the metrics of Fig. 2 (Figs. 1, Figs. S14-S18), we also include $R_{\Delta OA, \text{initial}}$ and
16 R_{age} for each metric of Fig. 2 sequentially removing one flight from the statistical analysis. These results are summarized in
17 Table S2. In general, removing single flights does not change our conclusions, particularly when correlations are moderate or
18 stronger. Scatter in $\Delta OA_{\text{initial}}$ leads to weaker R_{age} values than would be obtained if we normalized changes with aging to the
19 first (normalized) value. However, as plume-density-dependent aging prior to the first transect is one of the potentially
20 interesting findings of this study, we feel that it is important to not normalize our changes further. Figs. S13, S19-S22 show
21 the same details as Fig. 2 but provide sensitivity tests to our methodology. Figure S13 examines potential FIMS
22 measurement artifacts by only using data from the first 50% of each flight leg when particle concentrations are increasing,
23 which lessens response-time-artifacts of the FIMS during transitions from high to low concentration regions. Figure S20
24 tests our assumed in-plume CO threshold value by increasing it from 150 ppbv to 200 ppbv (Fig. S19). Figure S21 tests
25 ΔCO percentile spacing by changing the bins from 5-15%, 15-50%, 50-90%, and 90-100% to 5-25%, 25-75%, and 75-100%.
26 Figure S22 tests assumed background region by increasing data used from the lowest 10% to the lowest 25% of CO
27 measurements. Although these figures show slight variability, the findings discussed below remain robust, and we constrain
28 the rest of our discussion to the original assumptions made for the FIMS measurements, in-plume CO threshold value, and
29 ΔCO percentiles used in Fig. 2.

Deleted: how well variability

Deleted: can be predicted

Deleted: the

Formatted: Subscript

33 In general, both the cores and edges do not show any positive or negative trend in $\Delta\text{OA}/\Delta\text{CO}$ with respect to
 34 physical aging. The correlation coefficients, $R_{\Delta\text{OA},\text{initial}}$ and R_{age} , show very weak correlations of 0.02 and +0.03 (with
 35 $R_{\Delta\text{OA},\text{initial}}$ and R_{age} ranging between -0.25 to +0.17 and 0 to 0.07, respectively, when individual flights are left out
 36 sequentially; Table S2). The absolute variability in $\Delta\text{OA}/\Delta\text{CO}$ is dominated by differences between plumes. Many previous
 37 field campaigns similarly show little change in $\Delta\text{OA}/\Delta\text{CO}$ with aging (Hodshire et al., 2019a and references therein; Palm et
 38 al., 2020). This may be due to a balance between evaporation and condensation over the period of time that the plume is
 39 observed (Hodshire et al., 2019a). This hypothesis is supported by the observed Δf_{60} and Δf_{44} : The fractional components
 40 Δf_{60} and Δf_{44} show clear signs of changes with aging, consistent with previous studies (Cubison et al. 2011; May et al. 2015;
 41 Garofalo et al. 2019; Forrister et al. 2015; Lee et al. 2020). Δf_{60} generally decreases with plume age ($R_{\text{age}} = -0.26$; a weak
 42 correlation), consistent with the hypotheses that compounds containing species that can fragment to m/z 60 in the SP-AMS
 43 may be evaporating because of dilution, undergoing heterogeneous oxidation to new forms that do not appear at m/z 60,
 44 and/or having a decreasing fractional contribution due to condensation of other compounds. In contrast, Δf_{44} generally
 45 increases with age ($R_{\text{age}} = +0.5$; a moderate correlation) for all plumes with available data. It appears for the plumes in this
 46 study that although there is little change in $\Delta\text{OA}/\Delta\text{CO}$, loss of compounds such as those that contribute to f_{60} fragments (as
 47 captured by the SP-AMS) is roughly balanced by condensation of more-oxidized compounds, including those that contain
 48 compounds with f_{44} fragments, such as carboxylic acids. This observation also suggests the possibility of heterogeneous or
 49 particle-phase oxidation that would alter the balance of Δf_{60} and Δf_{44} . However, estimates of heterogeneous mass losses
 50 indicate that after three hours of aging (the range of time the BBOP measurements were taken in) for a range of OH
 51 concentrations and reactive uptake coefficients, less than 10% of aerosol mass is lost to heterogeneous reactions (Fig. S23;
 52 see SI text S2 for more details on the calculation). These calculations indicate that heterogeneous loss has limited effect on
 53 aerosol composition or mass. Hence, the evaporation of compounds that contribute to m/z 60 in the SP-AMS being balanced
 54 by gas-phase production of compounds that contribute to m/z 44 in the SP-AMS may be the more likely pathway. When
 55 individual flights are left out sequentially, R_{age} ranges from -0.21 to -0.38 and +0.4 to +0.57 for Δf_{60} and Δf_{44} , respectively
 56 (Table S2).

57 Two more important features of Δf_{60} and Δf_{44} can be seen within Fig. 2: (1) Δf_{60} and Δf_{44} depend on $\Delta\text{OA}_{\text{initial}}$
 58 (moderate correlations of $R_{\Delta\text{OA},\text{initial}} = +0.43$ and -0.55 , respectively), with plumes with higher $\Delta\text{OA}_{\text{initial}}$ having
 59 consistently higher Δf_{60} and lower Δf_{44} . (2) The differences in Δf_{60} and Δf_{44} are apparent even for the nearest-to-source
 60 measurements that are ~15 minutes after the time of emission. Prior studies have shown that f_{60} and f_{44} at the time of
 61 emissions correlate with OA emissions factors through variability in burn conditions (Hennigan et al. 2011; Cubison et al.
 62 2011; McClure et al. 2020), and this relationship might also contribute to our observed correlation between Δf_{60} and Δf_{44}
 63 with $\Delta\text{OA}_{\text{initial}}$. For this emissions relationship to be an important factor, the variability in the OA emission factor needs to be
 64 a significant contributor to the variability in $\Delta\text{OA}_{\text{initial}}$. The relative variability in the OA emission factor is much smaller than
 65 the relative variability in $\Delta\text{OA}_{\text{initial}}$, and other factors contributing to variability in $\Delta\text{OA}_{\text{initial}}$ will negate an emissions-based
 66 covariance between $\Delta\text{OA}_{\text{initial}}$ with Δf_{60} and Δf_{44} . While our observed $\Delta\text{OA}_{\text{initial}}$ in Figure 2 spans nearly a factor of 100,

Deleted: f60 and f44

Formatted: Subscript

Deleted: $\Delta\text{OA}_{\text{initial}}$

Deleted: f

Deleted: t

Deleted: $\Delta\text{OA}_{\text{initial}}$

Deleted: $\Delta\text{OA}_{\text{initial}}$

Deleted: $\Delta\text{OA}_{\text{initial}}$

Deleted: Δf_{60} and Δf_{44}

Deleted: $\Delta\text{OA}_{\text{initial}}$

76 Andreae (2019) shows that the OA emission factors have a -1σ to $+1\sigma$ range of around a factor 3. Hence, variability in fuel
 77 consumption rates and dilution prior to the first transect likely dominate the variability in $\Delta\text{OA}_{\text{initial}}$, and the relationships of
 78 Δf_{60} and Δf_{44} with $\Delta\text{OA}_{\text{initial}}$ are unlikely to be influenced much by variability in burn conditions. We conclude that
 79 evaporation and/or chemistry prior to the first measurement appears to drive the initial relationship between Δf_{60} and Δf_{44}
 80 with $\Delta\text{OA}_{\text{initial}}$, consistent with (1) the theoretical work of Hodshire et al. (2019a), (2) an analysis of what chemistry would be
 81 missed in laboratory experiments if the initial 10-60 minutes of chemistry was not considered, following field experiments
 82 (Hodshire et al., 2019b), and (3) recent field analysis indicating that up to one-third of primary OA from biomass burning
 83 evaporates and subsequently reacts to form biomass burning SOA (Palm et al. 2020). We include in the supporting
 84 information scatter plots of each parameter of Fig. 1 as a function of $\Delta\text{OA}_{\text{initial}}$ (Fig. S24), and observe no trends other than
 85 the cores of the plumes generally having a higher $\Delta\text{OA}_{\text{initial}}$ than the edges of the plumes, as expected. The amount of
 86 evaporation and/or chemistry appear to depend on $\Delta\text{OA}_{\text{initial}}$, with higher rates of evaporation and chemistry occurring for
 87 lower values of $\Delta\text{OA}_{\text{initial}}$. This result is consistent with the hypothesis that aircraft observations are missing evaporation and
 88 chemistry prior to the first aircraft observation (Hodshire et al., 2019b). The differences in $\Delta\text{OA}_{\text{initial}}$ between plumes may be
 89 due to different emissions fluxes (e.g., due to different fuels or combustion phases) or plume widths, where larger/thicker
 90 plumes dilute more slowly than smaller/thinner plumes. These larger plumes have been predicted to have less evaporation
 91 and may undergo relatively less photooxidation (Bian et al., 2017; Hodshire et al., 2019a, 2019b). When individual flights
 92 are left out sequentially, $R_{\Delta\text{OA}_{\text{initial}}}$ ranges from +0.3 to +0.58 and -0.42 to -0.63 for Δf_{60} and Δf_{44} , respectively (Table S2).

93 Garofalo et al. (2019) segregated smoke data from the WE-CAN field campaign by distance from the center of a
 94 given plume and showed that the edges of one of the fires studied have less fractional f_{60} and more fractional f_{44} (not
 95 background-corrected) than the core of the plume. Lee et al. (2020) saw similar patterns in a southwestern United States
 96 wildfire. Similarly, we find that the 730b flight shows a very similar pattern in f_{60} and f_{44} (Figs. S25-S26) to that shown in
 97 Fig. 6 of Garofalo et al. (2019). The 821b and 809a flights also hint at elevated f_{44} and decreased f_{60} at the edges but the
 98 remaining plumes do not show a clear trend from the physical edges to cores in f_{60} and f_{44} . This could be as CO
 99 concentrations (and thus presumably other species) do not evenly increase from the edge to the core for many of the plume
 100 transects studied (Figs. S2-S6). To more clearly see this, Fig. S27 provides the same style of figure as Figs. S26-S27 for in-
 101 plume CO concentrations. Generally CO peaks around the centerline and is highest in the most fresh transect, but shows
 102 variability across transects. We do not have UV measurements that allow us to calculate photolysis rates but the in-plume
 103 SPN1 shortwave measurements in the visible show a dimming in the fresh cores that has a similar pattern to f_{44} and the
 104 inverse of f_{60} (Fig. S28; the rapid oscillations in this figure could be indicative of sporadic cloud cover above the plumes).
 105 Lee et al. (2020) similarly saw indications of enhanced photochemical bleaching at the edges of a southwestern United States
 106 wildfire when examining aerosol optical properties.

107 We also plot core and edge $\Delta\text{H}/\Delta\text{C}$ and $\Delta\text{O}/\Delta\text{C}$ as a function of physical age (Fig. 2d-e). Similar to Δf_{44} , $\Delta\text{O}/\Delta\text{C}$
 108 increases with physical age and is moderately correlated to both physical age and $\Delta\text{OA}_{\text{initial}}$ (moderate correlations of $R_{\text{age}} = +$
 109 0.561 and $R_{\Delta\text{OA}_{\text{initial}}} = -0.45$). When individual flights are left out sequentially, R_{age} for $\Delta\text{O}/\Delta\text{C}$ ranges between +0.46 and

Deleted: σ

Deleted: σ

Deleted: Δf_{60} and Δf_{44}

Deleted: $\Delta\text{OA}_{\text{initial}}$

Deleted: Δf_{60} and Δf_{44}

Deleted: $\Delta\text{OA}_{\text{initial}}$

Deleted: well

17 +0.63 and $R_{\Delta OA_{initial}}$ ranges between -0.21 and -0.54 (Table S2). Given that $\Delta f_{t,t}$ and $\Delta O/\Delta C$ are both metrics for OA aging
18 (Sect. 2), it is unsurprising that we see similar trends between them. Conversely, $\Delta H/\Delta C$ is poorly correlated to physical age
19 and $\Delta OA_{initial}$.

20 Both physical age and $\Delta OA_{initial}$ appear to influence Δf_{60} , $\Delta f_{t,t}$, and $\Delta O/\Delta C$: oxidation reactions and evaporation
21 promoted by dilution occur with aging, and the extent of photochemistry and dilution should depend on plume thickness.
22 Being able to predict biomass burning aerosol aging parameters can provide a framework for interstudy-comparisons and can
23 aid in modeling efforts. We construct mathematical fits for predicting Δf_{60} , $\Delta f_{t,t}$, and $\Delta O/\Delta C$:

$$X = a \log_{10}(\Delta OA_{initial}) + b (\text{Physical age}) + c \quad \text{Eq. 4}$$

24
25
26 where X is Δf_{60} , $\Delta f_{t,t}$, or $\Delta O/\Delta C$, physical age is in hours, and a , b , and c are fit coefficients. The measured versus fit data are
27 shown in Fig. 3a-c. The values of a , b , and c are provided in Table S3. The Pearson and Spearman coefficients of
28 determination (R_p^2 and R_s^2 , respectively) are also summarized in Fig. 3 and indicate weak-moderate goodness of fits (R_p^2 and
29 R_s^2 of 0.28 and 0.25 for Δf_{60} , R_p^2 and R_s^2 of 0.58 and 0.6 for $\Delta f_{t,t}$, and R_p^2 and R_s^2 of 0.45 and 0.55 for $\Delta O/\Delta C$). We show R^2
30 here to indicate the fraction of variability captured by these fits, whereas calculating R for the trends in Fig. 2 indicate the
31 direction of the correlation. We do not constrain our fits to go through the origin. To provide further metrics of goodness-of-
32 fit, we also include the normalized mean bias (NMB) and normalized mean error (NME) in percent for each metric of Fig. 3.
33 The NMB values are very close to zero (which is anticipated as linear fits seek to minimize the sum of squared residuals).
34 The NME is larger, at 19.8% for Δf_{60} , 14.9% for $\Delta f_{t,t}$, and 10.2% for $\Delta O/\Delta C$. The p-values for each fit are less than 0.01.
35 Although no models that we are aware of currently predict aerosol fractional components (e.g. f_{60} or $f_{t,t}$), O/H and H/C are
36 predicted by some models (e.g., Cappa and Wilson (2012) and these fit parameters may assist in modeling of aging biomass
37 burning aerosol. Other functional forms for fits were explored, with the following form showing similar results as Eq. 4:
38

$$\ln(\Delta X) = a \ln(\Delta OA_{initial}) + b \ln(\text{Physical age}) + c \quad \text{Eq. 5}$$

39
40
41 (Fig. S29 and Table S4 for the fit coefficients) and $\Delta N_{initial}$ in the place of $\Delta OA_{initial}$ in Eq. 4 (Fig. S30 and Table S5 for the fit
42 coefficients) providing similar correlation values and NMB and NME values for Δf_{60} , $\Delta f_{t,t}$, and $\Delta O/\Delta C$.

43
44 The aging values of Δf_{60} , $\Delta f_{t,t}$, and $\Delta O/\Delta C$ show scatter in time (Figs. S14-18), which likely contributes to the
45 limited predictive power of our mathematical fits. The scatter is likely due to variability in emissions due to source fuel or
46 combustion conditions, instrument noise and responses under the large concentration ranges encountered in these smoke
47 plumes, inhomogeneous mixing within the plume, variability in background concentrations not captured by our background
48 correction method, inaccurate characterizations of physical age due to variable wind speed, and/or deviations from a true
49 Lagrangian flight path. Eqs. 4-5 performed the best out of the mathematical fits that we tested. These equations do not have a
50 direct physical interpretation due to their indirect relations to age and initial aerosol mass. But they may be used as a starting

Deleted: but

52 point for modeling studies as well as for constructing a more physically based fit. There may be another variable not
53 available to us in the BBOP measurements that can improve these mathematical fits, such as photolysis rates. We do not
54 know whether these fits may well-represent fires in other regions around the world, given variability in fuels and burn
55 conditions. We also do not know how these fits will perform under nighttime conditions, as our fits were made for daytime
56 conditions with different chemistry than would happen at night. We encourage these fits to be tested with further data sets
57 and modeling. These equations are a first step towards parameterizations appropriate for regional and global modeling and
58 need extensive testing to separate influences of oxidation versus dilution-driven evaporation.

59 3.2 Aerosol size distribution properties: $\Delta N/\Delta CO$ and \overline{D}_p

60 The observations of the normalized number concentration between 40-262 nm, $\Delta N/\Delta CO$ (Fig. 2f), show that plume
61 edges and cores generally show decreases in $\Delta N/\Delta CO$ with physical age, with a weak correlation of $R_{\text{age}} = -0.27$ (-0.13 to -
62 0.43 when individual flights are left out, sequentially; Table S2). Although we would anticipate that plume regions with
63 higher initial ΔOA would have lower normalized number concentrations due to coagulation (Sakamoto et al. 2016), a few
64 dense cores have normalized number concentrations comparable or higher than the thinner edges, leading to no correlation
65 with $\Delta OA_{\text{initial}}$. We note that variability in number emissions (e.g., due to burn conditions) adds unexplained variability not
66 captured by the R values.

67 The mean particle size between 40-262 nm, \overline{D}_p (Eq. 3), is shown to statistically increase with aging when
68 considered across the BBOP dataset (Fig. 2g) (a moderate correlation of $R_{\text{age}} = +0.53$, with R_{age} ranging between +0.43 to
69 +0.63 when individual flights are left out sequentially; Table S2). Coagulation and SOA condensation will increase \overline{D}_p . OA
70 evaporation will decrease \overline{D}_p if the particles are in quasi-equilibrium (where evaporation is independent of surface area)
71 (Hodshire et al. 2019b). However, if evaporation is kinetically limited, smaller particles will preferentially evaporate more
72 rapidly than larger particles, which may lead to an increase in \overline{D}_p if the smallest particles evaporate below 40 nm (Hodshire
73 et al. 2019b). The plumes do not show significant changes in $\Delta OA/\Delta CO$ (Fig. 2a), indicating that coagulation is likely
74 responsible for the majority of increases in \overline{D}_p . (We acknowledge that $\Delta OA/\Delta CO$ may be impacted by measurement artifacts
75 as discussed in Sect. 2. For instance, if the collection efficiency of the AMS is actually decreasing with age, then $\Delta OA/\Delta CO$
76 would be increasing and the increases in number mean diameter will be due to SOA condensation as well as coagulation.)
77 We do not have measurements for the volatility of the smoke aerosol, and so cannot refine these conclusions further. We also
78 perform the functional fit analysis following Sect. 3.1 (Eq. 4; where X is \overline{D}_p in this case). The fit can also predict greater than
79 30 percent of the variance in \overline{D}_p (R_p^2 and R_s^2 of 0.37 and 0.33, NME of 5.5%, and p-value less than 0.01; Fig. 3d) but does
80 not predict $\Delta N/\Delta CO$ well (not shown). We show the functional fit for \overline{D}_p for the alternative fit equation (Eq. 5) in Fig. S29
81 and Table S4. We also show the functional fit for \overline{D}_p for Eq. 4 with $\Delta N_{\text{initial}}$ in place of $\Delta OA_{\text{initial}}$ in Fig. 30 and Table S5.
82 Sakamoto et al. (2016) provide fit equations for modeled \overline{D}_p as a function of age, but they include a known initial \overline{D}_p at the
83 time of emission in their parameterization (rather than 15 minutes or greater, as available to us in this study), which is not

84 available here. $\Delta N_{\text{initial}}$ in the place of $\Delta \text{OA}_{\text{initial}}$ in Eq. 4 predicts \bar{D}_p similarly (Fig. S30). As discussed in Section 3.1, scatter
85 in number concentrations limits our prediction skill.

86 Particles appear in the 20-40 nm size range in the FIMS measurements independently of plume OA concentrations
87 (Figs S7-S11), implying that nucleation events may be occurring for some of the transects. Some pseudo-Lagrangian sets of
88 transects also show nucleation-mode particles downwind of fires in between transects (Figs. S7, S8, S9, and S11).
89 Nucleation-mode particles appear to be approximately one order of magnitude less concentrated than the larger particles, and
90 primarily occur in the outer portion of plumes, although one set of transects did show nucleation-mode particles within the
91 core of the plume (Fig. S11). Nucleation at edges could be due to increased photooxidation from higher total irradiance
92 relative to the core (Fig. S26). As well, nucleation is more favorable when the total condensation sink is lower (e.g. reduced
93 particle surface area; Dal Maso et al., 2002), which may occur for outer portions of plumes with little aerosol loading.
94 However, given the relatively small number of data points showing nucleation mode particles and limited photooxidation
95 and gas-phase information, we do not have confidence in the underlying source of the nucleation-mode particles.

96 4 Summary and outlook

97 The BBOP field campaign provided high time resolution (1 s) measurements of gas- and particle-phase smoke
98 measurements downwind of western U.S. wildfires along pseudo-Lagrangian transects. These flights have allowed us to
99 examine near-field (<4 hours) aging of smoke particles to provide analyses on how select species vary across a range of initial
00 organic aerosol mass loadings ($\Delta \text{OA}_{\text{initial}}$; a proxy for the relative rates at which the plume is anticipated to dilute as dilution
01 before the first observation is not a measurable quantity). **We have also examined** how the species studied vary between the
02 edges and cores of each plume. We find that although $\Delta \text{OA}/\Delta \text{CO}$ does not correlate with $\Delta \text{OA}_{\text{initial}}$ or physical age, Δf_{60} (a
03 marker for evaporation) is moderately correlated with $\Delta \text{OA}_{\text{initial}}$ (Spearman rank-order correlation tests correlation coefficient,
04 $R_{\Delta \text{OA}_{\text{initial}}}$, of +0.43) and weakly correlated with physical age (Spearman rank-order correlation tests correlation coefficient,
05 R_{age} , of -0.26). Δf_{44} and $\Delta \text{O}/\Delta \text{C}$ (markers for photochemical aging) increases with physical aging (moderate correlations of R_{age}
06 of +0.5 and +0.56, respectively) and are inversely related to $\Delta \text{OA}_{\text{initial}}$ (moderate correlations of $R_{\Delta \text{OA}_{\text{initial}}}$ of -0.55 and -0.45,
07 respectively). $\Delta N/\Delta \text{CO}$ decreases with physical aging, likely through coagulation. Mean aerosol diameter increases with age
08 primarily due to coagulation, as **normalized** organic aerosol mass does not change significantly, and is moderately correlated
09 with physical age ($R_{\text{age}} = +0.53$). Nucleation is observed within a few of the fires and appears to occur primarily on the edges
10 of the plumes. Differences in initial values of Δf_{60} , Δf_{44} , and $\Delta \text{O}/\Delta \text{C}$ are evidence that evaporation and/or chemistry has
11 occurred before the time of initial measurement and that plumes or plume regions with lower initial aerosol loading can undergo
12 these changes more rapidly than thicker plumes. We have developed fit equations that can weakly to moderately predict Δf_{60}
13, Δf_{44} , $\Delta \text{O}/\Delta \text{C}$, and mean aerosol diameter given a known initial (at the time of first measurement) total organic aerosol mass
14 loading and physical age. We were unable to quantify the impact on potential inter-fire variability in the emission values of
15 the metrics studied here (such as variable emissions of species that can contribute to m/z 60 and m/z 44). We anticipate that

Deleted: as well as

17 being able to capture this additional source of variability may lead to stronger fits and correlation. We encourage future studies
18 to attempt to quantify these chemical and physical changes before the initial measurement using combinations of modeling
19 and laboratory measurements, where sampling is possible at the initial stages of the fire and smoke. We also suggest further
20 refinement of our fit equations, as additional variables (such as photolysis rates) and better quantification of inter-fire
21 variability (such as variable emission rates) are anticipated to improve these fits. We finally urge future near-field (<24 hours)
22 analyses of recent and future biomass burning field campaigns to include differences in initial plume mass concentrations and
23 location within the plume as considerations for understanding chemical and physical processes in plumes.

24 **Acknowledgements**

25 We would like to thank Lauren Garofalo, Emily Fischer, Jakob Lindaas, and Ilana Pollack for useful conversations. We
26 thank Charles Long for use of irradiation data. This work is supported by the U.S. NOAA, an Office of Science, Office of
27 Atmospheric Chemistry, Carbon Cycle, and Climate Program, under the cooperative agreement awards NA17OAR4310001
28 and NA17OAR4310003; the U.S. NSF Atmospheric Chemistry program, under Grants AGS-1559607 and AGS-1950327;
29 and the US Department of Energy's (DOE) Atmospheric System Research, an Office of Science, Office of Biological and
30 Environmental Research program, under grant DE-SC0019000. Work conducted by LIK, AJS, JW was performed under
31 sponsorship of the U.S. DOE Office of Biological & Environmental Sciences (OBER) Atmospheric System Research
32 Program (ASR) under contracts DE-SC0012704 (BNL; LIK, AJS) and DE-SC0020259 (JW). Researchers recognize the
33 DOE Atmospheric Radiation Measurement (ARM) Climate Research program and facility for both the support to carry out
34 the BBOP campaign and for use of the G-1 research aircraft. TBO acknowledges support from the DOE ARM program
35 during BBOP and the DOE ASR program for BBOP analysis (contract DE-SC0014287). DKF acknowledges funding from
36 NOAA Climate Program Office's Atmospheric Chemistry, Carbon Cycle, and Climate program (Grant NA17OAR4310010).
37 We thank the anonymous reviewers for their constructive feedback.

38

39

40

41 **References**

42 Adachi, K., Sedlacek, A. J., Kleinman, L., Springston, S. R., Wang, J. and Chand, D.: Spherical tarball particles form
43 through rapid chemical and physical changes of organic matter in biomass-burning smoke, Proceedings of the
44 National Academy of Sciences, 1–6, 2019.

45 Aiken, A. C., Decarlo, P. F., Kroll, J. H., Worsnop, D. R., Huffman, J. A., Docherty, K. S., Ulbrich, I. M., Mohr, C.,
46 Kimmel, J. R., Sueper, D., Sun, Y., Zhang, Q., Trimborn, A., Northway, M., Ziemann, P. J., Canagaratna, M. R.,
47 Onasch, T. B., Alfarra, M. R., Prevot, A. S. H., Dommen, J., Duplissy, J., Metzger, A., Baltensperger, U. and
48 Jimenez, J. L.: O/C and OM/OC ratios of primary, secondary, and ambient organic aerosols with high-resolution
49 time-of-flight aerosol mass spectrometry, *Environmental Science and Technology*, 42(12), 4478–4485, 2008.

50 Aiken, A. C., Salcedo, D., Cubison, M. J., Huffman, J. A., DeCarlo, P. F., Ulbrich, I. M., Docherty, K. S., Sueper, D.,
51 Kimmel, J. R., Worsnop, D. R. and Others: Mexico City aerosol analysis during MILAGRO using high resolution
52 aerosol mass spectrometry at the urban supersite (T0)--Part I: Fine particle composition and organic source
53 apportionment, *Atmos. Chem. Phys.*, 9(17), 6633–6653, 2009.

54 Akagi, S. K., Yokelson, R. J., Wiedinmyer, C., Alvarado, M. J., Reid, J. S., Karl, T., Crounse, J. D. and Wennberg, P. O.:
55 Emission factors for open and domestic biomass burning for use in atmospheric models, *Atmos. Chem. Phys.*,
56 11(9), 4039–4072, 2011.

57 Akagi, S. K., Craven, J. S., Taylor, J. W., Mcmeeking, G. R., Yokelson, R. J., Burling, I. R., Urbanski, S. P., Wold, C. E.,
58 Seinfeld, J. H., Coe, H., Alvarado, M. J. and Weise, D. R.: Evolution of trace gases and particles emitted by a
59 chaparral fire in California, *Atmos. Chem. Phys.*, 12, 1397–1421, 2012.

60 Albrecht, B. A.: Aerosols, cloud microphysics, and fractional cloudiness, *Science*, 245(4923), 1227–1230, 1989.

61 Alfarra, M. R., Coe, H., Allan, J. D., Bower, K. N., Boudries, H., Canagaratna, M. R., Jimenez, J. L., Jayne, J. T., Garforth,
62 A. A., Li, S.-M. and Worsnop, D. R.: Characterization of urban and rural organic particulate in the Lower Fraser
63 Valley using two Aerodyne Aerosol Mass Spectrometers, *Atmos. Environ.*, 38(34), 5745–5758, 2004.

64 Andela, N., Morton, D. C., Giglio, L., Paugam, R., Chen, Y., Hantson, S., Werf, G. R. and Randerson, J. T.: The Global Fire
65 Atlas of individual fire size, duration, speed and direction, *Earth System Science Data*, 11(2), 529–552, 2019.

66 Andreae, M. O.: Emission of trace gases and aerosols from biomass burning – an updated assessment,
67 *Atmos. Chem. Phys.*, 19, 8523–8546, <https://doi.org/10.5194/acp-19-8523-2019>, 2019.

68 Badosa, J., Wood, J., Blanc, P., Long, C. N., Vuilleumier, L., Demengel, D. and Haefelin, M.: Solar irradiances measured
69 using SPN1 radiometers: uncertainties and clues for development, *Atmospheric Measurement Techniques*, 7, 4267–
70 4283, 2014.

71 Bian, Q., Jathar, S. H., Kodros, J. K., Barsanti, K. C., Hatch, L. E., May, A. A., Kreidenweis, S. M. and Pierce, J. R.:
72 Secondary organic aerosol formation in biomass-burning plumes: Theoretical analysis of lab studies and ambient
73 plumes, *Atmos. Chem. Phys.*, 17(8), 5459–5475, 2017.

74 Brito, J., Rizzo, L. V., Morgan, W. T., Coe, H., Johnson, B., Haywood, J., Longo, K., Freitas, S., Andreae, M. O. and
75 Artaxo, P.: Ground-based aerosol characterization during the South American Biomass Burning Analysis
76 (SAMBBA) field experiment, *Atmospheric Chemistry and Physics*, 14(22), 12069–12083, doi:10.5194/acp-14-
77 12069-2014, 2014.

78 Cachier, H., Liousse, C., Buat-Menard, P. and Gaudichet, A.: Particulate content of savanna fire emissions, *J. Atmos. Chem.*,
79 22(1-2), 123–148, 1995.

80 Canagaratna, M. R., Jimenez, J. L., Kroll, J. H., Chen, Q., Kessler, S. H., Massoli, P., Hildebrandt Ruiz, L., Fortner, E.,
81 Williams, L. R., Wilson, K. R. and Others: Elemental ration measurements of organic compounds using aerosol
82 mass spectrometry: characterization, improved calibration, and implications, *Atmos. Chem. Phys.*, 15, 253–272,
83 2015.

84 Capes, G., Johnson, B., McFiggans, G., Williams, P. I., Haywood, J. and Coe, H.: Aging of biomass burning aerosols over
85 West Africa: Aircraft measurements of chemical composition, microphysical properties, and emission ratios, *J.*
86 *Geophys. Res. D: Atmos.*, 113(23), 0–15, 2008.

87 Cappa, C. D. and Jimenez, J. L.: Quantitative estimates of the volatility of ambient organic aerosol, *Atmos. Chem. Phys.*,
88 10(12), 5409–5424, 2010.

89 Cappa, C. D. and Wilson, K. R.: Multi-generation gas-phase oxidation, equilibrium partitioning, and the formation and
90 evolution of secondary organic aerosol, *Atmos. Chem. Phys.*, 12(20), 9505–9528, 2012.

91 Carrico, C. M., Petters, M. D., Kreidenweis, S. M., Collett, J. L., Jr., Engling, G. and Malm, W. C.: Aerosol hygroscopicity
92 and cloud droplet activation of extracts of filters from biomass burning experiments, *J. Geophys. Res.*, 113(D8),
93 4767, 2008.

94 Canagaratna, M., Jayne, J., Jimenez, J., Allan, J., Alfarra, M., Zhang, Q., Onasch, T., Drewnick, F., Coe, H., Middlebrook,
95 A., Delia, A., Williams, L., Trimborn, A., Northway, M., DeCarlo, P., Kolb, C., Davidovits, P. and Worsnop, D.:
96 Chemical and microphysical characterization of ambient aerosols with the aerodyne aerosol mass spectrometer,
97 *Mass Spectrom. Rev.*, 26: 185-222. doi:10.1002/mas.20115, 2007

98
99
00
01
02

03 Chen, Q., Heald, C. L., Jimenez, J. L., Canagaratna, M. R., Qi, Z., Ling-Yan, H., Xiao-Feng, H., Campuzano-Jost, P., Palm,
04 B. B., Poulain, L., Kuwata, M., Martin, S. T., Ab-batt, J. P. D., Lee, A. K. Y., and Liggio, J.: Elemental
05 composition of organic aerosol: the gap between ambient and laboratory measurements, *Geophysical Research*
06 *Letters*, 42, 4182-4189, <https://doi.org/10.1002/2015gl063693>, 2015

07 Collier, S., Zhou, S., Onasch, T. B., Jaffe, D. A., Kleinman, L., Sedlacek, A. J., Briggs, N. L., Hee, J., Fortner, E., Shilling, J.
08 E., Worsnop, D., Yokelson, R. J., Parworth, C., Ge, X., Xu, J., Butterfield, Z., Chand, D., Dubey, M. K., Pekour, M.

09 S., Springston, S. and Zhang, Q.: Regional Influence of Aerosol Emissions from Wildfires Driven by Combustion
10 Efficiency: Insights from the BBOP Campaign, *Environmental Science and Technology*, 50(16), 8613–8622, 2016.

11 Collier, S., Williams, L. R., Onasch, T. B., Cappa, C. D., Zhang, X., Russell, L. M., Chen, C. L., Sanchez, K. J., Worsnop,
12 D. R. and Zhang, Q.: Influence of Emissions and Aqueous Processing on Particles Containing Black Carbon in a
13 Polluted Urban Environment: Insights From a Soot Particle-Aerosol Mass Spectrometer, *J. Geophys. Res. Atmos.*,
14 123(12), 6648–6666, doi:10.1002/2017JD027851, 2018.

15 Corbin, J. C., Lohmann, U., Sierau, B., Keller, A., Burtscher, H., and Mensah, A. A.: Black carbon surface oxidation and
16 organic composition of beech-wood soot aerosols, *Atmos. Chem. Phys.*, 15, 11885–11907,
17 <https://doi.org/10.5194/acp-15-11885-2015>, 2015.

18 Cubison, M. J., Ortega, A. M., Hayes, P. L., Farmer, D. K., Day, D., Lechner, M. J., Brune, W. H., Apel, E., Diskin, G. S.,
19 Fisher, J. A., Fuelberg, H. E., Hecobian, A., Knapp, D. J., Mikoviny, T., Riemer, D., Sachse, G. W., Sessions, W.,
20 Weber, R. J., Weinheimer, A. J., Wisthaler, A. and Jimenez, J. L.: Effects of aging on organic aerosol from open
21 biomass burning smoke in aircraft and laboratory studies, *Atmos. Chem. Phys.*, 11(23), 12049–12064, 2011.

22 Dal Maso, M., Kulmala, M., Lehtinen, K. E. J., Mäkelä, J. M., Aalto, P., and O'Dowd, C. D.: Condensation and coagulation
23 sinks and formation of nucleation mode particles in coastal and boreal forest boundary layers, *J. Geophys. Res.*,
24 107(D19), doi:10.1029/2001JD001053, 2002.

25 Decarlo, P. F., Dunlea, E. J., Kimmel, J. R., Aiken, A. C., Sueper, D., Crounse, J., Wennberg, P. O., Emmons, L., Shinozuka,
26 Y., Clarke, A., Zhou, J., Tomlinson, J., Collins, D. R., Knapp, D., Weinheimer, A. J., Montzka, D. D., Campos, T.
27 and Jimenez, J. L.: Fast airborne aerosol size and chemistry measurements above Mexico City and Central Mexico
28 during the MILAGRO campaign., 2008.

29 Dennison, P. E., Brewer, S. C., Arnold, J. D. and Moritz, M. A.: Large wildfire trends in the western United States, 1984-
30 2011, *Geophysical Research Letters*, 41(8), 2928–2933, doi:10.1002/2014gl059576, 2014.

31 Eatough, D. J., Eatough, N. L., Pang, Y., Sizemore, S., Kirchstetter, T. W., Novakov, T. and Hobbs, P. V.: Semivolatile
32 particulate organic material in southern Africa during SAFARI 2000, *J. Geophys. Res. D: Atmos.*, 108(D13)
33 [online] Available from:
34 [https://agupubs.onlinelibrary.wiley.com/doi/abs/10.1029/2002JD002296%4010.1002/%28ISSN%292169-](https://agupubs.onlinelibrary.wiley.com/doi/abs/10.1029/2002JD002296%4010.1002/%28ISSN%292169-8996.SAF1, 2003)
35 [8996.SAF1, 2003](https://agupubs.onlinelibrary.wiley.com/doi/abs/10.1029/2002JD002296%4010.1002/%28ISSN%292169-8996.SAF1, 2003).

36 Evans, J. D. (1996). *Straightforward statistics for the behavioral sciences*. Thomson Brooks/Cole Publishing Co.

37 Ford, B., Val Martin, M., Zelasky, S. E., Fischer, E. V., Anenberg, S. C., Heald, C. L. and Pierce, J. R.: Future Fire Impacts
38 on Smoke Concentrations, Visibility, and Health in the Contiguous United States, *GeoHealth*,
39 doi:10.1029/2018GH000144, 2018.

40 Formenti, P., Elbert, W., Maenhaut, W., Haywood, J., Osborne, S. and Andreae, M. O.: Inorganic and carbonaceous aerosols
41 during the Southern African Regional Science Initiative (SAFARI 2000) experiment: Chemical characteristics,
42 physical properties, and emission data for smoke from African biomass burning, *J. Geophys. Res. D: Atmos.*,
43 108(D13), doi:10.1029/2002JD002408, 2003.

44 Forrister, H., Liu, J., Scheuer, E., Dibb, J., Ziemba, L., Thornhill, K. L., Anderson, B., Diskin, G., Perring, A. E., Schwarz, J.
45 P., Campuzano-Jost, P., Day, D. A., Palm, B. B., Jimenez, J. L., Nenes, A. and Weber, R. J.: Evolution of brown
46 carbon in wildfire plumes, *Geophys. Res. Lett.*, 42(11), 4623–4630, 2015.

47 Gan, R. W., Ford, B., Lassman, W., Pfister, G., Vaidyanathan, A., Fischer, E., Volckens, J., Pierce, J. R. and Magzamen, S.:
48 Comparison of wildfire smoke estimation methods and associations with cardiopulmonary-related hospital
49 admissions, *GeoHealth*, 1(3), 122–136, 2017.

50 Garofalo, L., Pothier, M. A., Levin, E. J. T., Campos, T., Kreidenweis, S. M. and Farmer, D. K.: Emission and Evolution of
51 Submicron Organic Aerosol in Smoke from Wildfires in the Western United States, *ACS Earth and Space*
52 *Chemistry*, acsearthspacechem.9b00125, 2019.

53 Giglio, L., Csizsar, I. and Justice, C. O.: Global distribution and seasonality of active fires as observed with the Terra and
54 Aqua Moderate Resolution Imaging Spectroradiometer (MODIS) sensors, *Journal of Geophysical Research: Biogeosciences*,
55 111(G2) [online] Available from:
56 <https://agupubs.onlinelibrary.wiley.com/doi/abs/10.1029/2005JG000142>, 2006.

57 Giglio, L., Csizsar, I., Restás, Á., Morissette, J. T., Schroeder, W., Morton, D. and Justice, C. O.: Active fire detection and
58 characterization with the advanced spaceborne thermal emission and reflection radiometer (ASTER), *Remote*
59 *Sensing of Environment*, 112(6), 3055–3063, doi:10.1016/j.rse.2008.03.003, 2008.

60 Gilman, J. B., Lerner, B. M., Kuster, W. C., Goldan, P. D., Warneke, C., Veres, P. R., Roberts, J. M., De Gouw, J. A.,
61 Burling, I. R. and Yokelson, R. J.: Biomass burning emissions and potential air quality impacts of volatile organic
62 compounds and other trace gases from fuels common in the US, *Atmos. Chem. Phys.*, 15(24), 13915–13938, 2015.

63 Grieshop, A. P., Logue, J. M., Donahue, N. M., and Robinson, A. L.: Laboratory investigation of photochemical oxidation of
64 organic aerosol from wood fires 1: measurement and simulation of organic aerosol evolution, *Atmos. Chem. Phys.*,
65 9, 1263–1277, <https://doi.org/10.5194/acp-9-1263-2009>, 2009.

66 Hatch, L. E., Luo, W., Pankow, J. F., Yokelson, R. J., Stockwell, C. E. and Barsanti, K. C.: Identification and quantification
67 of gaseous organic compounds emitted from biomass burning using two-dimensional gas chromatography-time-of-
68 flight mass spectrometry, *Atmos. Chem. Phys.*, 15(4), 1865–1899, 2015.

69 Hatch, L. E., Yokelson, R. J., Stockwell, C. E., Veres, P. R., Simpson, I. J., Blake, D. R., Orlando, J. J. and Barsanti, K. C.:
70 Multi-instrument comparison and compilation of non-methane organic gas emissions from biomass burning and
71 implications for smoke-derived secondary organic aerosol precursors, *Atmos. Chem. Phys.*, 17, 1471–1489, 2017.

72 Heald, C. L., Kroll, J. H., Jimenez, J. L., Docherty, K. S., DeCarlo, P. F., Aiken, A. C., Chen, Q., Martin, S. T., Farmer, D.
73 K. and Artaxo, P.: A simplified description of the evolution of organic aerosol composition in the atmosphere,
74 *Geophys. Res. Lett.*, 37(8), doi:10.1029/2010GL042737, 2010.

75 Hecobian, A., Liu, Z., Hennigan, C. J., Huey, L. G., Jimenez, J. L., Cubison, M. J., Vay, S., Diskin, G. S., Sachse, G. W.,
76 Wisthaler, A., Mikoviny, T., Weinheimer, A. J., Liao, J., Knapp, D. J., Wennberg, P. O., Urten, A., Crouse, J. D.,
77 Clair, J. S., Wang, Y. and Weber, R. J.: Comparison of chemical characteristics of 495 biomass burning plumes

78 intercepted by the NASA DC-8 aircraft during the ARCTAS/CARB-2008 field campaign, *Atmos. Chem. Phys.*, 11,
79 13325–13337, 2011.

80 Hennigan, C. J., Miracolo, M. A., Engelhart, G. J., May, A. A., Presto, A. A., Lee, T., Sullivan, A. P., McMeeeking, G. R.,
81 Coe, H., Wold, C. E., Hao, W. M., Gilman, J. B., Kuster, W. C., De Gouw, J., Schichtel, B. A., Collett, J. L.,
82 Kreidenweis, S. M. and Robinson, A. L.: Chemical and physical transformations of organic aerosol from the photo-
83 oxidation of open biomass burning emissions in an environmental chamber, *Atmos. Chem. Phys.*, 11(15), 7669–
84 7686, doi:10.5194/acp-11-7669-2011, 2011.

85 Hobbs, P. V., Sinha, P., Yokelson, R. J., Christian, T. J., Blake, D. R., Gao, S., Kirchstetter, T. W., Novakov, T. and
86 Pilewskie, P.: Evolution of gases and particles from a savanna fire in South Africa, *J. Geophys. Res. D: Atmos.*,
87 108(D13), doi:10.1029/2002JD002352, 2003.

88 Hodshire, A. L., Akherati, A., Alvarado, M. J., Brown-Steiner, B., Jathar, S. H., Jimenez, J. L., Kreidenweis, S. M.,
89 Lonsdale, C. R., Onasch, T. B., Ortega, A. M. and Pierce, J. R.: Aging Effects on Biomass Burning Aerosol Mass
90 and Composition: A Critical Review of Field and Laboratory Studies, *Environ. Sci. Technol.*, 53(17), 10007–
91 10022, 2019a.

92 Hodshire, A. L., Bian, Q., Ramnarine, E., Lonsdale, C. R., Alvarado, M. J., Kreidenweis, S. M., Jathar, S. H. and Pierce, J.
93 R.: More than emissions and chemistry: Fire size, dilution, and background aerosol also greatly influence near-field
94 biomass burning aerosol aging, *J. Geophys. Res. D: Atmos.*, 2018JD029674, 2019b.

95 Huffman, J. A., Docherty, K. S., Aiken, A. C., Cubison, M. J., Ulbrich, I. M., Decarlo, P. F., Sueper, D., Jayne, J. T.,
96 Worsnop, D. R., Ziemann, P. J. and Jimenez, J. L.: Chemically-resolved aerosol volatility measurements from two
97 megacity field studies., 2009.

98 Janhäll, S., Andreae, M. O. and Pöschl, U.: Biomass burning aerosol emissions from vegetation fires: particle number and
99 mass emission factors and size distributions, *Atmos. Chem. Phys. Disc.*, 9(4), 17183–17217, 2009.

00 Jen, C. N., Hatch, L. E., Selimovic, V., Yokelson, R. J., Weber, R., Fernandez, A. E., Kreisberg, N. M., Barsanti, K. C. and
01 Goldstein, A. H.: Speciated and total emission factors of particulate organics from burning western US wildland
02 fuels and their dependence on combustion efficiency, *Atmos. Chem. Phys.*, 19, 1013–1026, 2019.

03 Jimenez, J. L., Canagaratna, M. R., Donahue, N. M., Prevot, a. S. H., Zhang, Q., Kroll, J. H., DeCarlo, P. F., Allan, J. D.,
04 Coe, H., Ng, N. L., Aiken, a. C., Docherty, K. S., Ulbrich, I. M., Grieshop, a. P., Robinson, a. L., Duplissy, J.,
05 Smith, J. D., Wilson, K. R., Lanz, V. a., Hueglin, C., Sun, Y. L., Tian, J., Laaksonen, A., Raatikainen, T.,
06 Rautiainen, J., Vaattovaara, P., Ehn, M., Kulmala, M., Tomlinson, J. M., Collins, D. R., Cubison, M. J., Dunlea, E.
07 J., Huffman, J. a., Onasch, T. B., Alfarra, M. R., Williams, P. I., Bower, K., Kondo, Y., Schneider, J., Drewnick, F.,
08 Borrmann, S., Weimer, S., Demerjian, K., Salcedo, D., Cottrell, L., Griffin, R., Takami, A., Miyoshi, T.,
09 Hatakeyama, S., Shimono, A., Sun, J. Y., Zhang, Y. M., Dzepina, K., Kimmel, J. R., Sueper, D., Jayne, J. T.,
10 Herndon, S. C., Trimborn, a. M., Williams, L. R., Wood, E. C., Middlebrook, a. M., Kolb, C. E., Baltensperger, U.
11 and Worsnop, D. R.: Evolution of organic aerosols in the atmosphere, *Science*, 326(5959), 1525–1529, 2009.

12 Jolleys, M. D., Coe, H., McFiggans, G., Capes, G., Allan, J. D., Crosier, J., Williams, P. I., Allen, G., Bower, K. N., Jimenez,
13 J. L., Russell, L. M., Grutter, M. and Baumgardner, D.: Characterizing the aging of biomass burning organic aerosol
14 by use of mixing ratios: A meta-analysis of four regions, *Environmental Science and Technology*, 46(24), 13093–
15 13102, 2012.

16 Jolleys, M. D., Coe, H., McFiggans, G., Taylor, J. W., O’Shea, S. J., Le Breton, M., Bauguitte, S. J. B., Moller, S., Di Carlo,
17 P., Aruffo, E., Palmer, P. I., Lee, J. D., Percival, C. J. and Gallagher, M. W.: Properties and evolution of biomass
18 burning organic aerosol from Canadian boreal forest fires, *Atmos. Chem. Phys.*, 15(6), 3077–3095, 2015.

19 Kleinman, L. I., Daum, P. H., Lee, Y. N., Senum, G. I., Springston, S. R., Wang, J., Berkowitz, C., Hubbe, J., Zaveri, R. A.,
20 Brechtel, F. J., Jayne, J., Onasch, T. B. and Worsnop, D.: Aircraft observations of aerosol composition and ageing
21 in New England and Mid-Atlantic States during the summer 2002 New England Air Quality Study field campaign,
22 *J. Geophys. Res. Atmos.*, 112(9), 1–18, doi:10.1029/2006JD007786, 2007.

23 Kleinman, L. and Sedlacek, A. J., III: Biomass Burning Observation Project (BBOP) Final Campaign Report, 2016.

24 Kleinman, L. I., Sedlacek, A. J., III, Adachi, K., Buseck, P. R., Collier, S., Dubey, M., K., Hodshire, A. L., Lewis, E.,
25 Onasch, T. B., Pierce, J. R., Schilling, J., Springston, S. R., Wang, J., Zhang, Q., Zhou, S., Yokelson, R. J.: Rapid
26 Evolution of Aerosol Particles and their Optical Properties Downwind of Wildfires in the Western U.S., submitted
27 to *Atmos. Chem. Phys.*, 2020.

28 Konovalov, I. B., Beekmann, M., Golovushkin, N. A. and Andreae, M. O.: Nonlinear behavior of organic aerosol in biomass
29 burning plumes: a microphysical model analysis, *Atmos. Chem. Phys. Disc.*, 1–44, 2019.

30 Koss, A. R., Sekimoto, K., Gilman, J. B., Selimovic, V., Coggon, M. M., Zarzana, K. J., Yuan, B., Lerner, B. M., Brown, S.
31 S., Jimenez, J. L., Krechmer, J., Roberts, J. M., Warneke, C., Yokelson, R. J. and De Gouw, J.: Non-methane
32 organic gas emissions from biomass burning: Identification, quantification, and emission factors from PTR-ToF
33 during the FIREX 2016 laboratory experiment, *Atmos. Chem. Phys.*, 18(5), 3299–3319, 2018.

34 Kroll, J. H. and Seinfeld, J. H.: Chemistry of secondary organic aerosol: Formation and evolution of low-volatility organics
35 in the atmosphere, *Atmos. Environ.*, 42, 3593–3624, 2008.

36 Kulkarni, P. and Wang, J.: New fast integrated mobility spectrometer for real-time measurement of aerosol size
37 distribution—I: Concept and theory, *J. Aerosol Sci.*, 37(10), 1303–1325, 2006.

38 Lee, J. E., Dubey, M. K., Aiken, A. C., Chylek, P., & Carrico, C. M.: Optical and chemical analysis of absorption
39 enhancement by mixed carbonaceous aerosols in the 2019 Woodbury, AZ fire plume, *J. Geophys. Res. Atmos.*,
40 125, e2020JD032399. <https://doi.org/10.1029/2020JD032399>, 2020.

41 Lee, T., Sullivan, A. P., Mack, L., Jimenez, J. L., Kreidenweis, S. M., Onasch, T. B., Worsnop, D. R., Malm, W., Wold, C.
42 E., Hao, W. M. and Collett, J. L.: Chemical Smoke Marker Emissions During Flaming and Smoldering Phases of
43 Laboratory Open Burning of Wildland Fuels, *Aerosol Sci. Technol.*, 44(9), i–v, 2010.

44 Lim, C. Y., Hagan, D. H., Coggon, M. M., Koss, A. R., Sekimoto, K., de Gouw, J., Warneke, C., Cappa, C. D., and Kroll, J.
45 H.: Secondary organic aerosol formation from the laboratory oxidation of biomass burning emissions, 920 Atmos.
46 Chem. Phys., 19, 12797-12809, 10.5194/acp-19-12797-2019, 2019.

47 Liu, X., Zhang, Y., Huey, L. G., Yokelson, R. J., Wang, Y., Jimenez, J. L., Campuzano-Jost, P., Beyersdorf, A. J., Blake, D.
48 R., Choi, Y., St. Clair, J. M., Crounse, J. D., Day, D. A., Diskin, G. S., Ried, A., Hall, S. R., Hanisco, T. F., King, L.
49 E., Meinardi, S., Mikoviny, T., Palm, B. B., Peischl, J., Perring, A. E., Pollack, I. B., Ryerson, T. B., Sachse, G.,
50 Schwarz, J. P., Simpson, I. J., Tanner, D. J., Thornhil, K. L., Ullmann, K., Weber, R. J., Wennberg, P. O.,
51 Wisthaler, A., Wolfe, G. M. and Ziemba, L. D.: Agricultural fires in the southeastern U.S. during SEAC4RS:
52 Emissions of trace gases and particles and evolution of ozone, reactive nitrogen, and organic aerosol, J. Geophys.
53 Res., 121(12), 7383–7414, 2016.

54 Liu, P.S.K., Deng, R., Smith, K.A., Williams, L.R., Jayne, J.T., Canagaratna, M.R., Moore, K., Onasch, T.B., Worsnop,
55 D.R., and Deshler, T.: Transmission Efficiency of an Aerodynamic Focusing Lens System: Comparison of Model
56 Calculations and Laboratory Measurements for the Aerodyne Aerosol Mass Spectrometer, Aerosol Sci. Technol.,
57 41(8):721–733, 2007 Long, C. N., Bucholtz, A., Jonsson, H., Schmid, B., Vogelmann, A. and Wood, J.: A Method
58 of Correcting for Tilt from Horizontal in Downwelling Shortwave Irradiance Measurements on Moving Platforms,
59 The Open Atmospheric Science Journal, 4(1), 78–87, doi:10.2174/1874282301004010078, 2010.

60 Massoli, P., Onasch, T. B., Cappa, C. D., Nuamaan, I., Hakala, J., Hayden, K., Li, S., Sueper, D. T., Bates, T. S., Quinn, P.
61 K., Jayne, J. T., and Worsnop, D. R.: Characterization of black carbon-containing particles from soot particle
62 aerosol mass spectrometer measurements on the R/V Atlantis during CalNex 2010. J. Geophys. Res. Atmos., 120,
63 2575– 2593. doi: 10.1002/2014JD022834, 2015.

64 May, A. A., Levin, E. J. T., Hennigan, C. J., Riipinen, I., Lee, T., Collett, J. L., Jimenez, J. L., Kreidenweis, S. M. and
65 Robinson, A. L.: Gas-particle partitioning of primary organic aerosol emissions: 3. Biomass burning, J. Geophys.
66 Res. D: Atmos., 118(19), 11327–11338, 2013.

67 May, A. A., Lee, T., McMeeking, G. R., Akagi, S., Sullivan, A. P., Urbanski, S., Yokelson, R. J. and Kreidenweis, S. M.:
68 Observations and analysis of organic aerosol evolution in some prescribed fire smoke plumes, Atmos. Chem. Phys.,
69 15(11), 6323–6335, 2015.

70 McClure, C. D., Lim, C. Y., Hagan, D. H., Kroll, J. H., and Cappa, C. D.: Biomass-burning-derived particles from a wide
71 variety of fuels – Part 1: Properties of primary particles, Atmos. Chem. Phys., 20, 1531-1547,
72 <https://doi.org/10.5194/acp-20-1531-2020>, 2020.

73 Middlebrook, A. M., Bahreini, R., Jimenez, J. L. and Canagaratna, M. R.: Evaluation of composition-dependent collection
74 efficiencies for the Aerodyne aerosol mass spectrometer using field data, Aerosol Sci. Technol., 46(3), 258–271,
75 doi:10.1080/02786826.2011.620041, 2012.

76 Morgan, W. T., Allan, J. D., Bauguitte, S., Darbyshire, E., Flynn, M. J., Lee, J., Liu, D., Johnson, B., Haywood, J., Longo,
77 K. M., Artaxo, P. E. and Coe, H.: Transformation and aging of biomass burning carbonaceous aerosol over tropical

78 South America from aircraft in-situ measurements during SAMBBA, *Atmos. Chem. Phys. Discuss.*,
79 doi:10.5194/acp-2019-157, 2019.

80 Moteki, N. and Kondo, Y.: Dependence of Laser-Induced Incandescence on Physical Properties of Black Carbon Aerosols:
81 Measurements and Theoretical Interpretation, *Aerosol Sci. Technol.*, 44(8), 663–675, 2010.

82 Nance, J. D., Hobbs, P. V. and Radkel, L. F.: Airborne Measurements of Gases and Particles From an Alaskan Wildfire, *J.*
83 *Geophys. Res. D: Atmos.*, 98(D8), 873–882, 1993.

84 Noyes, K. J., Kahn, R., Sedlacek, A., Kleinman, L., Limbacher, J. and Li, Z.: Wildfire Smoke Particle Properties and
85 Evolution, from Space-Based Multi-Angle Imaging, *Remote Sensing*, 12(5), 769, doi:10.3390/rs12050769, 2020.

86 O'Dell, K., Ford, B., Fischer, E. V. and Pierce, J. R.: Contribution of Wildland-Fire Smoke to US PM_{2.5} and Its Influence
87 on Recent Trends, *Environmental Science & Technology*, 53(4), 1797–1804, doi:10.1021/acs.est.8b05430, 2019.

88 Olfert, J. S. and Wang, J.: Dynamic Characteristics of a Fast-Response Aerosol Size Spectrometer, *Aerosol Sci. Technol.*,
89 43(2), 97–111, 2009.

90 Onasch, T. B., Trimborn, A., Fortner, E. C., Jayne, J. T., Kok, G. L., Williams, L. R., Davidovits, P. and Worsnop, D. R.:
91 Soot Particle Aerosol Mass Spectrometer: Development, Validation, and Initial Application, *Aerosol Science and*
92 *Technology*, 46(7), 804–817, doi:10.1080/02786826.2012.663948, 2012.

93 Palm, B. B., Peng, Q., Fredrickson, C. D., Lee, B. H., Garofalo, L. A. and Pothier, M. A.: Quantification of organic aerosol
94 and brown carbon evolution in fresh wildfire plumes, , doi:10.1073/pnas.2012218117, 2020.

95 Petters, M. D. and Kreidenweis, S. M.: A single parameter representation of hygroscopic growth and cloud condensation
96 nucleus activity, *Atmos. Chem. Phys.*, 7(8), 1961–1971, 2007.

97 Petters, M. D., Carrico, C. M., Kreidenweis, S. M., Prenni, A. J., DeMott, P. J., Collett, J. L. and Moosmüller, H.: Cloud
98 condensation nucleation activity of biomass burning aerosol, *J. Geophys. Res. D: Atmos.*, 114(22), 22205, 2009.

99 Ramnarine, E., Kodros, J. K., Hodshire, A. L., Lonsdale, C. R., Alvarado, M. J. and Pierce, J. R.: Effects of near-source
00 coagulation of biomass burning aerosols on global predictions of aerosol size distributions and implications for
01 aerosol radiative effects, *Atmos. Chem. Phys.*, 19(9), 6561–6577, 2019.

02 Reid, C. E., Brauer, M., Johnston, F. H., Jerrett, M., Balmes, J. R. and Elliott, C. T.: Critical review of health impacts of
03 wildfire smoke exposure, *Environmental Health Perspectives*, 124(9), 1334–1343, doi:10.1289/ehp.1409277, 2016.

04 Reid, J. S., Hobbs, P. V., Ferek, R. J., Blake, D. R., Martins, J. V., Dunlap, M. R. and Lioussé, C.: Physical, chemical, and
05 optical properties of regional hazes dominated by smoke in Brazil, *J. Geophys. Res. D: Atmos.*, 103(D24), 32059–
06 32080, 1998.

07 Reid, J. S., Eck, T. F., Christopher, S. A., Koppmann, R., Dubovik, O., Eleuterio, D. P., Holben, B. N., Reid, E. A. and
08 Zhang, J.: A review of biomass burning emissions part III: intensive optical properties of biomass burning particles,
09 *Atmos. Chem. Phys.*, 5, 827–849, 2005.

10 Sakamoto, K. M., Allan, J. D., Coe, H., Taylor, J. W., Duck, T. J. and Pierce, J. R.: Aged boreal biomass-burning aerosol
11 size distributions from BORTAS 2011, *Atmos. Chem. Phys.*, 15(4), 1633–1646, 2015.

12 Sakamoto, K. M., Laing, J. R., Stevens, R. G., Jaffé, D. A. and Pierce, J. R.: The evolution of biomass-burning aerosol size
13 distributions due to coagulation: Dependence on fire and meteorological details and parameterization, *Atmos.*
14 *Chem. Phys.*, 16(12), 7709–7724, 2016.

15 Schwarz, J. P., Gao, R. S., Fahey, D. W., Thomson, D. S., Watts, L. A., Wilson, J. C., Reeves, J. M., Darbeheshti, M.,
16 Baumgardner, D. G., Kok, G. L. and Others: Single-particle measurements of midlatitude black carbon and light-
17 scattering aerosols from the boundary layer to the lower stratosphere, *J. Geophys. Res. D: Atmos.*, 111(D16)
18 [online] Available from: <https://agupubs.onlinelibrary.wiley.com/doi/abs/10.1029/2006JD007076>, 2006.

19 Schwarz, J.P., Spackman, J.R., Gao, R.S., Perring, a. E., Cross, E., Onasch, T.B., Ahern, a., Wrobel, W., Davidovits, P.,
20 Olfert, J., Dubey, M.K., Mazzoleni, C., and Fahey, D.W.:The Detection Efficiency of the Single Particle Soot
21 Photometer, *Aerosol Sci. Technol.*, 44(8):612–628, 2010. Sedlacek, A. J., Iii, Buseck, P. R., Adachi, K., Onasch, T.
22 B., Springston, S. R. and Kleinman, L.: Formation and evolution of Tar Balls from Northwestern US wildfires,
23 *Atmos. Chem. Phys. Discuss.*, (Figure 1), 1–28, 2018.

24 Seinfeld, J. H. and Pandis, S. N.: *Atmospheric chemistry and physics: From air pollution to climate change*, John Willey &
25 Sons, Inc. , New York, 2006.

26

27 Shrivastava, M., Cappa, C. D., Fan, J., Goldstein, A. H., Guenther, A. B., Jimenez, J. L., Kuang, C., Laskin, A., Martin, S.
28 T., Ng, N. L. and Others: Recent advances in understanding secondary organic aerosol: Implications for global
29 climate forcing, *Rev. Geophys.*, 55(2), 509–559, 2017.

30 Spracklen, D. V., Mickley, L. J., Logan, J. A., Hudman, R. C., Yevich, R., Flannigan, M. D. and Westerling, A. L.: Impacts
31 of climate change from 2000 to 2050 on wildfire activity and carbonaceous aerosol concentrations in the western
32 United States, *J. Geophys. Res.*, 114(D20), 1418, 2009.

33 Tang, X., Madronich, S., Wallington, T. and Calamari, D.: Changes in tropospheric composition and air quality, *J.*
34 *Photochem. Photobiol. B*, 46(1-3), 83–95, 1998.

35 Tie, X.: Effect of clouds on photolysis and oxidants in the troposphere, *J. Geophys. Res.*, 108(D20), 23,073, 2003.

36 Twomey, S.: Pollution and the planetary albedo, *Atmos. Environ.*, 8(12), 1251–1256, 1974.

37 Vakkari, V., Kerminen, V.-M., Beukes, J. P., Titta, P., van Zyl, P. G., Josipovic, M., Wnter, A. D., Jaars, K., Worsnop, D.
38 R., Kulmala, M. and Laakso, L.: Rapid changes in biomass burning aerosols by atmospheric oxidation, *Geophys.*
39 *Res. Lett.*, 2644–2651, 2014.

40 Vakkari, V., Beukes, J. P., Dal Maso, M., Aurela, M., Josipovic, M. and van Zyl, P. G.: Major secondary aerosol formation
41 in southern African open biomass burning plumes, *Nat. Geosci.*, 11(8), 580–583, 2018.

42 Volkamer, R., Jimenez, J. L., San Martini, F., Dzepina, K., Zhang, Q., Salcedo, D., Molina, L. T., Worsnop, D. R. and
43 Molina, M. J.: Secondary organic aerosol formation from anthropogenic air pollution: Rapid and higher than
44 expected, *Geophys. Res. Lett.*, 33(17), 4407, 2006.

45 Volkamer, R., Ziemann, P. J. and Molina, M. J.: Secondary Organic Aerosol Formation from Acetylene (C₂H₂): seed effect
46 on SOA yields due to organic photochemistry in the aerosol aqueous phase, *Atmos. Chem. Phys.*, 9(6), 1907–1928,
47 2009.

48 Wang, J., -N. Lee, Y., Daum, P. H., Jayne, J. and Alexander, M. L.: Effects of aerosol organics on cloud condensation
49 nucleus (CCN) concentration and first indirect aerosol effect, *Atmospheric Chemistry and Physics*, 8(21), 6325–
50 6339, doi:10.5194/acp-8-6325-2008, 2008.

51 Willis, M. D., Lee, A. K. Y., Onasch, T. B., Fortner, E. C., Williams, L. R., Lambe, A. T., Worsnop, D. R., and Abbatt, J. P.
52 D.: Collection efficiency of the soot-particle aerosol mass spectrometer (SP-AMS) for internally mixed particulate
53 black carbon, *Atmos. Meas. Tech.*, 7, 4507–4516, <https://doi.org/10.5194/amt-7-4507-2014>, 2014.

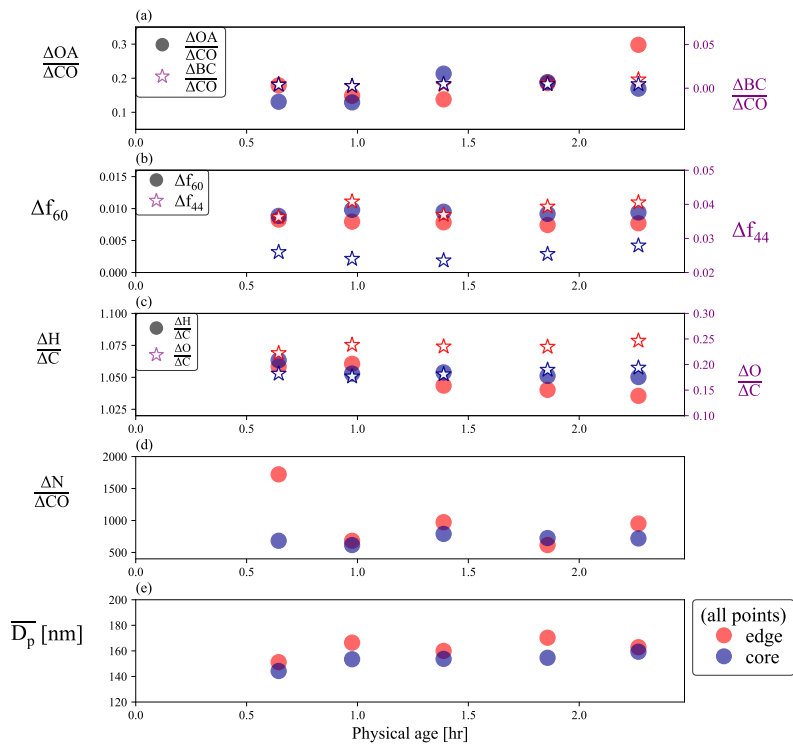
54 Yang, M., Blomquist, B. W. and Huebert, B. J.: Constraining the concentration of the hydroxyl radical in a stratocumulus-
55 topped marine boundary layer from sea-to-air eddy covariance flux measurements of dimethylsulfide, *Atmos.*
56 *Chem. Phys.*, 9(23), 9225–9236, 2009.

57 Yokelson, R. J., Crouse, J. D., DeCarlo, P. F., Karl, T., Urbanski, S., Atlas, E., Campos, T., Shinozuka, Y., Kapustin, V.,
58 Clarke, A. D., Weinheimer, A., Knapp, D. J., Montzka, D. D., Holloway, J., Weibring, P., Flocke, F., Zheng, W.,
59 Toohey, D., Wennberg, P. O., Wiedinmyer, C., Mauldin, L., Fried, A., Richter, D., Walega, J., Jimenez, J. L.,
60 Adachi, K., Buseck, P. R., Hall, S. R. and Shetter, R.: Emissions from biomass burning in the Yucatan, *Atmos.*
61 *Chem. Phys.*, 9(15), 5785–5812, 2009.

62 Yue, X., Mickley, L. J., Logan, J. A. and Kaplan, J. O.: Ensemble projections of wildfire activity and carbonaceous aerosol
63 concentrations over the western United States in the mid-21st century, *Atmospheric Environment*, 77, 767–780,
64 doi:10.1016/j.atmosenv.2013.06.003, 2013.

65 Zhou, S., Collier, S., Jaffe, D. A., Briggs, N. L., Hee, J., Sedlacek, A. J., III, Kleinman, L., Onasch, T. B. and Zhang, Q.:
66 Regional influence of wildfires on aerosol chemistry in the western US and insights into atmospheric aging of
67 biomass burning organic aerosol, *Atmos. Chem. Phys.*, 17(3), 2477–2493, 2017.

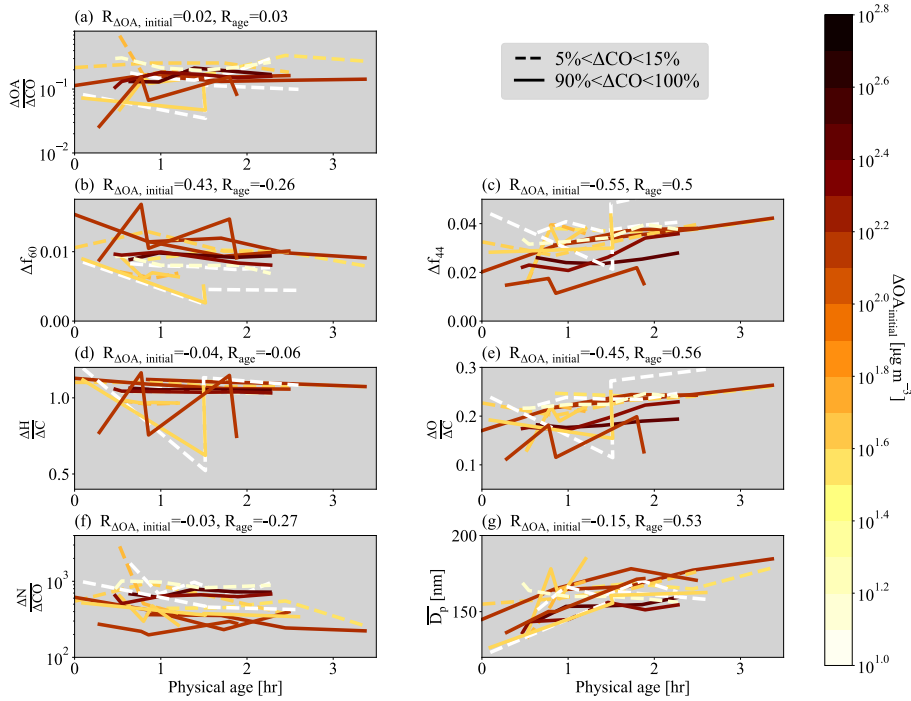
68
69
70
71
72
73
74



75

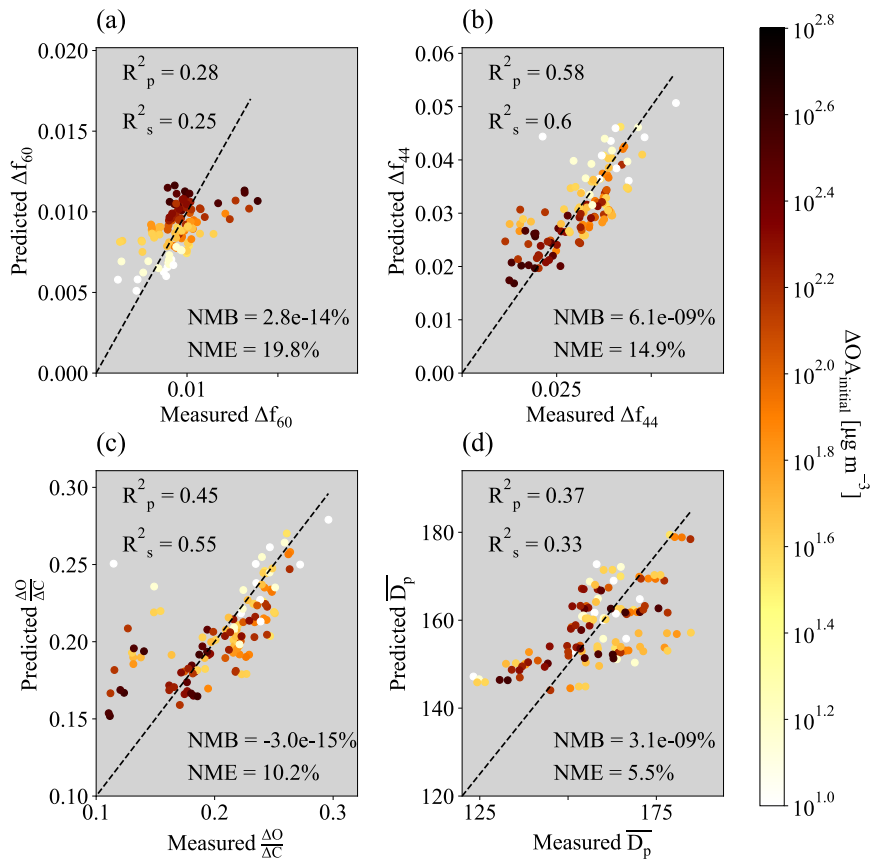
76 **Figure 1:** Aerosol properties from the first set of pseudo-Lagrangian transects from the Colockum fire on flight '730b' (a) $\Delta OA/\Delta CO$
 77 (right y-axis) and $\Delta BC/\Delta CO$ (left y-axis), (b) Δf_{60} (right y-axis) and Δf_{44} (left y-axis), (c) $\Delta H/\Delta C$ (right y-axis) and $\Delta O/\Delta C$ (left y-
 78 axis), (d) $\Delta N/\Delta CO$, and (e) $\overline{D_p}$ against physical age. For each transect, the data is divided into edge (the lowest 5-15% of ΔCO data;
 79 red points) and core (90-100% of ΔCO data; blue points).

80



81
82
83
84
85
86
87
88
89
90
91

Figure 2. Various normalized parameters as a function of physical age for the 7 sets of pseudo-Lagrangian transects. Separate lines are shown for the edges (lowest 5-15% of ΔCO ; dashed lines) and cores (highest 90-100% of ΔCO ; solid lines). (a) $\Delta OA / \Delta CO$, (b) Δf_{60} , (c) Δf_{44} , (d) $\Delta H / \Delta C$, (e) $\Delta O / \Delta C$, (f) $\Delta N / \Delta CO$, and (g) \overline{D}_p between 40-262 nm against physical age for all flights, colored by $\Delta OA_{initial}$. Some flights have missing data. Also provided is the Spearman correlation coefficient, R , between each variable and $\Delta OA_{initial}$ and physical age for each variable. Note that panels (a) and (f) have a log y-axis.



92
 93 **Figure 3.** Measured versus predicted (a) Δf_{60} , (b) Δf_{44} , (c) $\Delta O/\Delta C$, and (d) \overline{D}_p between 40-262 nm. The predicted values are from
 94 the equation $X = a \log_{10}(O A_{\text{initial}}) + b$ (Physical age) + c where $X = \Delta f_{60}$, Δf_{44} , $\Delta O/\Delta C$, or \overline{D}_p . The values of a, b, and c are provided in
 95 Table S3. The Pearson and Spearman coefficients of determination (R_p^2 and R_s^2 , respectively) are provided in each panel, along
 96 with the normalized mean bias (NMB) and normalized mean error (NME). Note that Fig. 2 provides R values rather than R^2 to
 97 provide information upon the trend of the correlation. Included in the fit and figure are points from all four ΔCO regions within
 98 the plume (the 5-15%, 15-50%, 50-90%, and 90-100% of ΔCO), all colored by the mean $\Delta O_{\text{initial}}$ of each ΔCO percentile range.
 99